NTNU

Norwegian University of
Science and Technology

Improved Petrophysical Evaluation of a Thinly Bedded Oil and Gas Bearing Reservoir, Using Triaxial Resistivity and Nuclear Magnetic Resonance Well Logging Measurements

Susanne Gryte Olsen

Petroleum Geoscience and Engineering
Submission date: June 2016
Supervisor: Erik Skogen, IPT

Norwegian University of Science and Technology
Department of Petroleum Engineering and Applied Geophysics

Abstract

The aim of this thesis was to conduct a petrophysical analysis on a laminated thin bedded reservoir from well 7220/8-1, containing gas in the upper section. A conventional analysis was done in advance, in order to create a basic zonation and an analysis of the logs available. The well was in addition compared with log data from two wells from the same area, 7220/7-1 and 7220/5-1, in order to see similarities and differences and correct for zonation within the two main reservoir formations, Stø and Nordmela.

Due to the conductive shale laminations masking the more resistive, hydrocarbon (HC) filled sand layers in the laminated reservoir sections, a method for calculation of corrected resistivity for the coarse grained layers (R_{cg}) was carried out. This method applied both NMR T2 distributions as indications for shale and sand fractions, and triaxial resistivities (Shray and Borbas, 2001).

As the reservoir contained gas, a new porosity was carried out in order to correct for both density and NMR porosities, which provided inaccurate values. A method combining both density and NMR porosities into one equation, called the Density Magnetic Resonance (DMR) method was applied to the dataset (Freedman et al., 1998).

In order to do a quality check of the zones interpreted as clean sand, laminated shaly sand, dispersed shaly sand and shales, Thomas-Stieber diagrams were created. DMR and density porosity vs. gamma ray was plotted, and an interpretation of the zonation was performed based on endpoints for clean sand, shale and dispersed shale. A summary was done as a final result by applying a corrected water saturation, calculated from R_{cg} and DMR, as input. This resulted in a HC pore thickness for each zone, which was multiplied with the sand volume and summed together as a total thickness for the reservoir.

The R_{cg} resistivity carried out showed good correlation with the vertical resistivity in the reservoir, and hence an elevated value in the laminated HC zones of the reservoir. This result is considered as more accurate within the coarse grained zones, due to the actual resistivity within the sand laminas being considerably higher than the averaged parallel measurements from the apparent resistivity curve (R_t). The results calculated from the DMR method showed excellent correlation with core porosities within the gas zone and throughout the whole reservoir interval. The DMR porosity equation corrected for both the elevated density porosity and the reduced NMR porosity.

The Thomas-Stieber diagrams provided plots that displayed a distribution of points from the assumed laminated zones around the laminated line, and the clean zones around the endpoints on the plot. No dispersed shale zone was indicated from the plot, and Archie's equation was therefore applied to all zones for saturation and summary calculations. The final summary result provided a total hydrocarbon pore thickness of 22.8 m within the reservoir section of 120.0 m.

Sammendrag

Målet med denne masteroppgaven var å utføre en petrofysisk analyse av et laminert sand-skifer reservoar fra brønn 7220/8-1, lokalisert i Barentshavet. Reservoaret består av tynne bergartslag, også kalt «thin beds», med innhold av både gass og olje. En konvensjonell analyse ble utført som første steg for å kunne dele inn loggene i soner og utføre en grunnleggende tolkning. Brønnen ble i tillegg sammenlignet med to andre brønner fra samme område, 7220/7-1 og 7220/5-1, for å se likheter og forskjeller i de to reservoarformasjonene, Stø og Nordmela.

På grunn av skiferens ledningsevne og parallelle resistivitetsmålinger, ble de resistive, hydrokarbonfylte sandlagene i de laminerte seksjonene av reservoaret maskert på den konvensjonelle resistivitetsloggen (R_t) og en korrigert resistivitet for de grovkornede lagene (R_{cg}) ble derfor regnet ut. Denne metoden tok i bruk NMR T2-distribusjoner som indikasjon for skifer- og sandvolumer, i tillegg til triaksiale resistivitetsmålinger (Shray and Borbas, 2001).

Ettersom reservoaret inneholdt gass, ble en ny porøsitet regnet ut i den hensikt å korrigere for både tetthets- og NMR-porøsiteter, som gav ut unøyaktige målerverdier. En fremgangsmåte som kombinerer både responsligningen for tetthet- og NMR-porøsitet inn i en ligning, ble anvendt. Metoden kalles «the Density Magnetic Resonance Method» (DMR) og har som hensikt å korrigere for gasseffekter som påvirker porøsistetslogger (Freedman et al., 1998).

Thomas-Stieber diagrammer ble laget for å utføre en kvalitetssjekk av sonene tolket som ren sand, laminert og dispergert skifrig sand, og skifer. Både DMR- og tetthetsporøsitet ble plottet sammen med gammastråleloggen og en tolkning av litologien i soneinndelingen ble utført basert på endepunkter for ren sand, skifer og dispergert skifer.

En oppsummeringskalkulasjon ble utført som et endelig resultat ved å bruke korrigert vannmetning, beregnet fra R_{cg} og DMR resultater, som inndata. Dette resulterte i en hydrokarbon-poretykkelse for hver enkelt sone, som ble multiplisert med sandvolum og til slutt summert sammen til en total tykkelse.

Resistiviteten som ble beregnet for de grovkornede reservoar-lagene (R_{cg}) viste en god korrelasjon med den vertikale resistiviteten i reservoaret. Dette er ansett som mer nøyaktig i de laminerte sonene, da den egentlige resistiviteten i sandlaminasjonene ville vært betydelig høyere enn de gjennomsnittlige, parallelle målingene fra R_t. Resultatene fra DMR-beregningen viste utmerket korrelasjon med porøsiteten målt fra kjerneprøver i gassonen. Denne porsøsitetsligningen korrigerte for både forhøyet tettehetsporøsitet og den reduserte NMR-porøsiteten.

Thomas-Stieber diagrammene indikerte at de tolkede laminerte sand-skifersonene og de rene sandsonene var korrekt inndelt. Diagrammene viste ingen tegn til dispergerte skifersoner og beregning av vannmetning for hele reservoaret ble derfor utført ved bruk av Archies ligning. Total hydrokarbon-poretykkelse ble beregnet til 22.8 meter i reservoaret med en høyde på 120.0 meter.

Acknowledgement

This thesis was written for the Department of Petroleum Engineering and Applied Geophysics (IPT) at the Norwegian University of Science and Technology (NTNU), in the spring of 2016.

I would like to thank Schlumberger for Techlog software support and Yngve Bolstad Johansen for assistance with NMR field print interpretation. I would also like to thank my fellow students for support and motivating study breaks during the semester.

Last, but not least I would like to give my acknowledgements to my supervisor, Assistant Professor Erik Skogen for excellent supervision and for providing me with well data. I would also like to thank him for his patience with answering all my questions throughout the semester and for sharing his valuable experience and knowledge with me.

Trondheim, June 9th, 2016

Susanne Gryte Olsen

Table of Contents

List of Figures

List of Tables

1. Introduction

Worldwide, 30-40 % of the in-place resources are confined within thin beds. Because of that, it is important to find their true potential with minimum uncertainty. Thin-bedded layers of silt and clay within a hydrocarbon bearing sand reservoir usually have a high irreducible water saturation, which means that the reservoir can produce oil and gas with zero water-cut (Tyagi et al., 2008).

Hydrocarbons are non-conductive and can easily be separated from conductive brine on resistivity logs within clean formations. When thin-beds of both sand and shale are present in a hydrocarbon filled reservoir, high resistivity intervals can be masked by conductive shales, and occur as low resistivity pay zones. When dealing with laminated thin beds of shale and sand, Archie's equation is considered the best approach for calculation of water saturation because the potential reservoir exist in clean sand beds within the formation. To use Archie's equation, correct resistivity and porosity measurement are needed. As the conductive shale beds will make the conventional resistivity tool measure a lower resistivity than reality, a more advanced tool can be applied to solve for this problem, by providing triaxial measurements and detecting anisotropy (Anderson et al., 2008).

Gas is common in reservoir sections, and a factor that complicates wellbore logging due to incorrect measurements of density and porosity. Gas present in the pore space affects the density tool to measure a lower density, and the NMR tool to measure a greater density, than the actual formation density. To correct for these effects, a method for more accurate porosity estimation can be applied, combining both response equations for density and NMR porosities (Freedman et al., 1998).

NMR and triaxial resistivity data is the key parameters in this thesis. NMR data provides valuable pore size data due to its sensitivity to the pore fluids, while the triaxial data will provide vertical resistivity and anisotropy indications, which will lead to a better thin-bed evaluation and a more accurate resistivity result for the sand beds. Corrected porosity and resistivity will together lead to a more accurate calculation of water and oil saturations in the thin-bedded reservoir sections.

This thesis will focus on the theory behind and the methods used for calculation of accurate resistivity and porosity in the reservoir found in well 7220/8-1 in the Barents Sea, containing thin beds with gas in the upper section. The methods used are mainly based on NMR and

triaxial resistivity data, in addition to conventional logs. Well 7220/8-1 is also compared with two nearby wells, in order to improve the zonation and interpretation of hydrocarbon intervals and lithology.

2. Background and Theory

2.1 Geological Setting and Well Information

Three wells from the Johan Castberg field in Barents Sea are introduced in this thesis. All wells are in the area of the Bjørnøya fault complex and penetrate through different segments of the Skrugard fault block. Location of the wells can be seen in Figure 1.

The reservoirs are discovered within two formations of Jurassic age, Stø and Nordmela. The lithostratigraphy for the Norwegian Barents Sea, containing the two formations, can be observed in Figure 2.

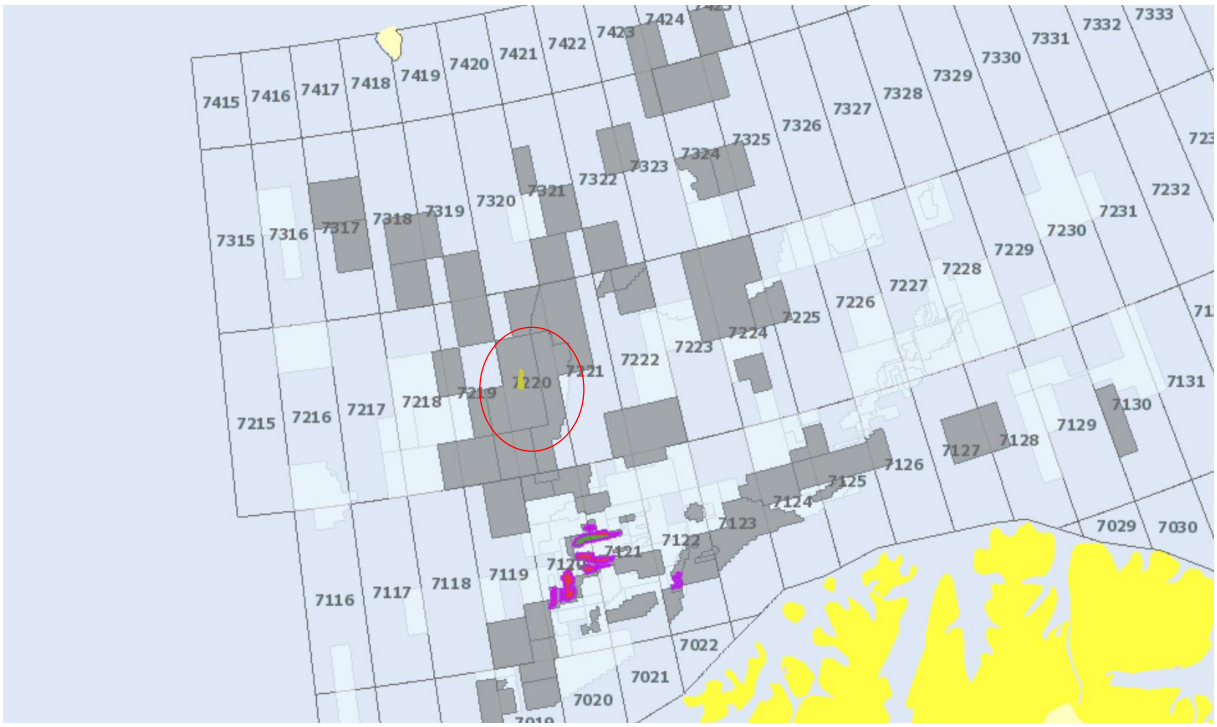

Figure 1 Map of the area around the wells interpreted in the Barents Sea, quadrant 7220 (NPD, 2016a).

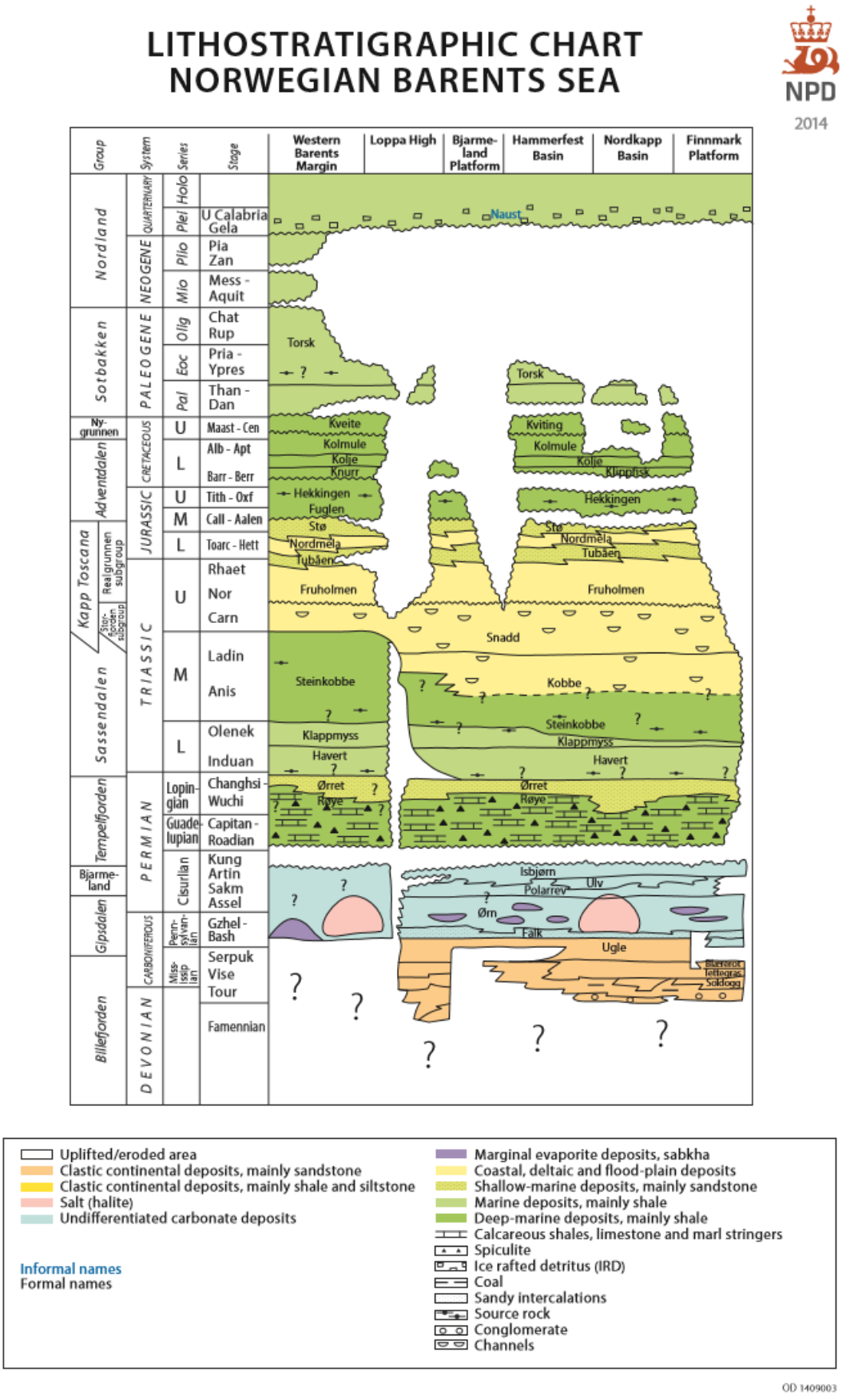

Figure 2 Lithostratigrafic chart of the Norwegian Barents Sea (NPD, 2014).

2.1.1 Stø Formation (FM)

The main lithology within the Stø FM is moderately to well-sorted sandstones containing thin units of siltstones and shales, deposited in programing costal regimes. The thin layers of siltstones and shale represents transgressive pulses. The formation is of Jurassic age, extending from Late Pliensbachian to Bajocian. From the wells drilled, the formation is found to be thickest in the south-west and thinning towards east. The formation consists of three different depositional sequences defined by transgressive episodes (NPD, 2016c):

- The basal sequence.
- The middle sequence, representing maximum transgression.
- The uppermost sequence, showing indications of syn-depositional uplift and erosion.

2.1.2 Nordmela Formation (FM)

The Nordmela formation consists of interbedded siltstones, sandstones, shales and clays with minor coals. The sandstone becomes more common in the top section of the formation. The depositional environment of the formation is tidal flats to flood plains, where the sandstone sequences represents estuarine and tidal channels. The formation is of Jurassic age, extending from Sinemurian to late Pliensbachian (NPD, 2016b).

2.1.3 Well 7220/8-1

The exploration well 7220/8-1 is located north of the Snøhvit field in the Barents Sea. The well penetrates through southern segment of the rotated Skrugard fault block. A reservoir package containing the Stø, Nordmela and Tubåen formations of Jurassic age, and Fruholmen and Snadd formations of Triassic age, occurs in the well. Great hydrocarbon shows were seen when drilling the primary target reservoir, top Stø Formation and top Nordmela, containing a 37 m thick gas column and an 83 m thick oil column.

A total of five cores were cut in the Stø and Nordmela Formations, in the interval 1292.5 - 1405.5 m. From seismic and well logging results, the GOC is set to 1312.0 m and the OWC is set to 1395.0 m. The total measured depth (MD) of well 7220/8-1 is at 2222.0 m (NPD, 2016f)

2.1.4 Well 7220/7-1

The exploration well 7220/7-1 is located southwest of well 7220/8-1, west of the Loppa high. The purpose of the well was to test hydrocarbon potential in the Jurassic formations Stø, Nordmela and Tubåen, and to test the sandstones in lower Fruholmen formation of Triassic age. The well had a MD at 2230.0 m and the Top Stø formation was found to be at 1781.0 m. Flat events on seismic correlated good with the GOC at 1828.0 m and OWC at 1956.0 m, found when logging the well.

Seven core plugs were cut out from the formations in the reservoir section and the water zone. Comprehensive wire line logging was conducted to the well (NPD, 2016e).

2.1.5 Well 7220/5-1

The appraisal well 7220/5-1 is located in the middle segment of the Skrugard discovery, west of the Loppa high. The well was drilled with the purpose of delineate the reservoir discovered in the Skrugard middle segment, and proving more accurate depths of OWC and OGC. The well was drilled to a total, measured and vertical (TVD), depth of 1740.0 m in the Fruholmen formation.

Above the reservoir, the wells penetrates through Tertiary and Cretaceous claystones and sandstones, in addition claystones from Late Jurassic. The Stø formation is found in the top reservoir at 1337.0 m. Inside the Stø formation, a 28 m thick gas column and a 47 m thick oil column were discovered. Results were in a good correlation with flat spots on seismic surveys, and proved a GOC at 1365.0 m and an OWC at 1412.0 m. Eight cores were provided from the well (NPD, 2016d) .

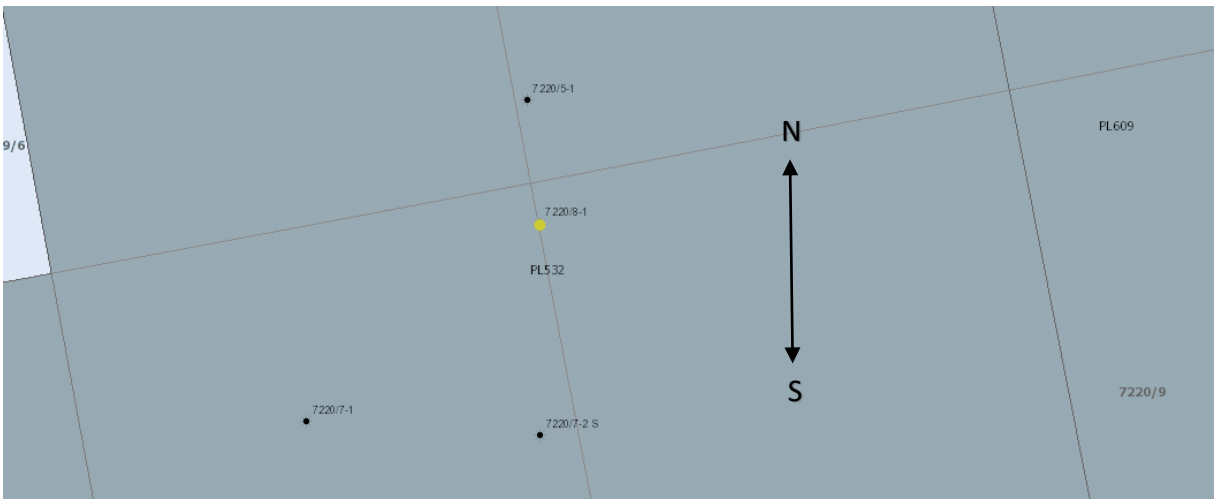

Figure 3 Locations of well 7220/8-1, 7220/7-1 and 7220/5-1 in the Barents Sea (NPD, 2016a).

2.2 Shaly Formations

Shale has a great impact on porosity and permeability measurements, and is one of the most important rocks in log analysis. Due to the shales electrical properties, it is also a good indicator for determination of fluid saturations in a rock matrix.

Shale is a mixture of different minerals of clay size, but often contains a large amount of clay minerals. The mixture of different minerals with different properties makes the shale anisotropic. The structure of the clay minerals are called sheets, and contain ions and cations (positive ions), which makes it a conductive material. These cations are attached to the surface of the clay sheets and provides a positive surface charge. This charged surface is often measured in terms of millions equivalents per 100 grams of dry clay minerals, and leads to the result of cations exchange capacity (CEC).

For water saturation calculations related to rock resistivity, Archie's equation is widely used. This equation is based on the assumption that water is the only conductive material in a formation, and does not take into account that the presence of other conductive materials, such as shale, can occur. If this is the case, the equation needs to be modified or a new model needs to be developed.

Clay minerals also complicates the porosity definitions of a rock. Each clay particle has a surface with bound water that is a part of the rocks pore space. This pore space is not included in the effective porosity and can therefore not work as a reservoir for hydrocarbons. In other words; shale can have a high total porosity, but at the same time a relatively low effective porosity because of the clays bound water (Schlumberger, 1989, pp. 8.13 - 8.15).

Depending on the amount of shale and its physical properties, the log readings from a tool may be affected. How the shale is distributed in the formation is also an important factor. Figure 4 shows how the shale distributions when divided into three main forms:

1. Laminar shale.
2. Structural shale.
3. Dispersed shale.

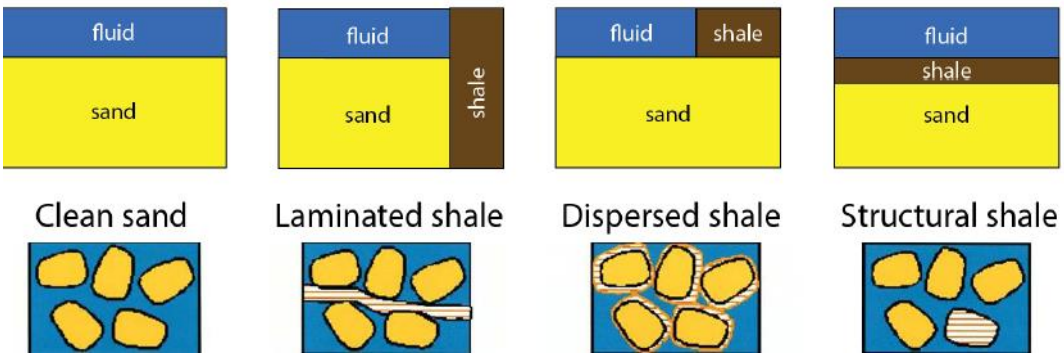

Figure 4 Forms of shale classified by manner of distribution in formation (Brandsen, 2016).

2.2.1 Laminar Shale

Shale distributed in thin layers between layers of sand, is called laminar shale. This form of dispersion can affect the average effective porosity in the formation, if the number of shale laminas increase as the pore medium is decreased. In general the shale laminas will not decrease porosity or permeability in the sand layers and is one of the better forms of dispersion in terms of reservoir quality (Schlumberger, 1989, pp. 8.13 - 8.15).

2.2.2 Structural Shale

Shale distributed as grains in the rock matrix is called structural shale. This form of dispersion will have properties similar to laminar shales and will not decrease the effective porosity or permeability. The original fluid volume will maintain the same and only grains will be replaced (Schlumberger, 1989, pp. 8.13 - 8.15).

2.2.3 Dispersed Shale

Shale distributed throughout the sand, filling up the space between the sand grains, is called dispersed shale. The dispersed shale can fill up the smaller pore channels and replace pore fluids, which again leads to a decrease in effective porosity and permeability of the formation. This form of shale distribution is not suitably in terms of reservoir quality (Schlumberger, 1989, pp. 8.13 - 8.15).

2.3 Resistivity

Resistivity is the ability of material to resist electrical conduction and is measured in ohm-m. The resistivity can be defined as a property of the material, but is at the same time dependent on the volume that is measured. Resistivity in boreholes can be achieved by wireline logging tools measuring the formation resistivity. The first resistivity tool developed for wireline logging was an electrode based measuring method, which acquired conductive mud in the borehole. In the 1940s the induction tool was introduced. This tool had the ability to measure the formation resistivity in non-conductive paths, such as oil based mud (Anderson et al., 2008).

Induction logging tools provide apparent resistivity from a large volume beyond the borehole. This type of measurement takes all of the components in the measured volume into account, which in turn influences the final result. This can in some cases have a negatively impact on the quality and the accuracy of the measurements, such as when the layers in the logging zone are non-perpendicular to the tool axis. In dipping beds and deviated wells, the presence of conductive layers will affect the resistivity in a way that can provide a lower resistivity value, which again might underestimate the hydrocarbons in place. The tool response can also be affected by heterogeneity between layers and electrical anisotropy. These effects, among others, needs to be corrected to obtain a useful resistivity result. Manual corrections were formerly used before computer based methods, as forward modelling and inversion, were developed to obtain a better approximation to the true resistivity value (Anderson et al., 2008).

The traditional uniaxial induction tool works well in vertical wells containing thick, homogenous beds. The tool is able to measure the apparent resistivity (R_a), in the horizontal plane, which is equivalent to horizontal resistivity (R_h), but does not have the ability to derive vertical resistivity (R_v).

According to Anderson et al., the physics of a uniaxial induction resistivity measurement can be demonstrated by a two- coil array, receiver and transmitter. An electromagnetic (EM) field is created in the formation, which causes currents to flow in a circular path around the tool, creating measurements in the horizontal direction. The currents ground loops are perpendicular to the tool's axis and concentric with the circular borehole. The phase and magnitude are dependent on the mud's conductivity. The current flowing in the ground loop creates its own electromagnetic (EM) field, which again induces voltage into the receiver coil. The formation resistivity that is measured is obtained from this voltage, and is known as the R-signal.

Commutation from voltage to conductivity can be done by the Biot-Savart law, or by a simplified model of the Maxwell equations (Anderson et al., 2008).

The ground loops are intersecting a large volume of the formation, which again provides an average apparent resistivity from several layers with different electrical properties. The anisotropy of the measurement will show a result dependent on the measuring direction of the tool. The anisotropy can be defined as R_v/R_h. Anisotropy will increase with increasing ratio of the two resistivities (Anderson et al., 2008).

2.3.1 The Triaxial RT Scanner Tool

The theoretical concept of the triaxial induction tool was first devised in the 1960s. Due to the technology limitations at that time, the tool was never developed. The interest of the tool increased as a consequence of the uniaxial tool's limitations. Both anisotropic areas and non-perpendicular bedding planes could be corrected for with a uniaxial measurement. In time, new technology appeared and methods for solving the problems that had been with the uniaxial tool was developed. This lead to the invention of the triaxial tool. This tool had some limitations, one of them being high sensitivity to the conductive mud. The formation signal from the borehole could be overwhelmed because of sensitivity, up to two magnitudes greater than for the uniaxial tool

Electrical anisotropy is a difficult formation property for the uniaxial induction tool to solve. This is common in laminated sand-shale sequences, which often can occur is reservoir intervals. The induction logging tool has a certain vertical resolution which implies that the laminas would need to have certain thickness in order to be detected. Beds that are thinner than the vertical resolution of the tool will be measured as an average of the properties of the individual layers, with the lowest resistivity dominating. From the article written by Anderson, B, et al. (2008), thin beds are by definition reservoir layers that are thinner than the vertical resolution of the tool (<1 ft, 0,3 m) (Anderson et al., 2008).

The triaxial tool measures all nine possible components of the resistivity, both parallel and perpendicular (vertical) to the shale-sand layers. The vertical method measures the laminations in series, and keeps its resistivity to the reservoir laminas by reducing the resistivity observed in thinly-bedded formations (Tyagi et al., 2008).

Triaxial resistivity is obtained by a RT scanner tool that has the ability to measure in three dimensions (x,y,z). The measurements are similar to the ones done by the uniaxial tool, but much more complex. The RT scanner tool consists of collocated triaxial transmitter array, three short axial receivers and three collocated triaxial receiver arrays. The transmitter coil generates magnetic moments in x, y and z directions. The receiver arrays for each direction is cross coupled to the two other directions, in addition to a direct coupling to its own transmitter array. This gives three measurements for each direction (see Figure 5), which are measured simultaneously. In order to obtain anisotropy, bed boundaries positions and dip from tensor voltage matrix, an advanced inversion is applied to the data. When the transmitters or receivers are placed at different positions, the cross couplings will be different to the direct couplings, and the coils needs to be collocated in order to get the right spacing. This is especially important for beds that are non-perpendicular of the tool's position (Anderson et al., 2008) .

The RT Scanner tool is able to solve for dipping beds and deviations in the well at the same time as it provides 3D measurements at different depths of investigation. The 3D measurements assure that the low resistivity effects from heterogeneous formations not affect the final result. An electrode sleeve with short single-axis and collocated triaxial receivers is used to fully characterize the borehole signal and remove borehole effect. R_v and R_h are determined using a 1D inversion algorithm (Schlumberger 2009). The main goal with the triaxial measurements is to apply R_v and R_h in calculations to obtain a more accurate water saturation (S_w). This enhanced S_w can be used to provide a more estimation of the hydrocarbons present in a thin-bedded reservoir section.

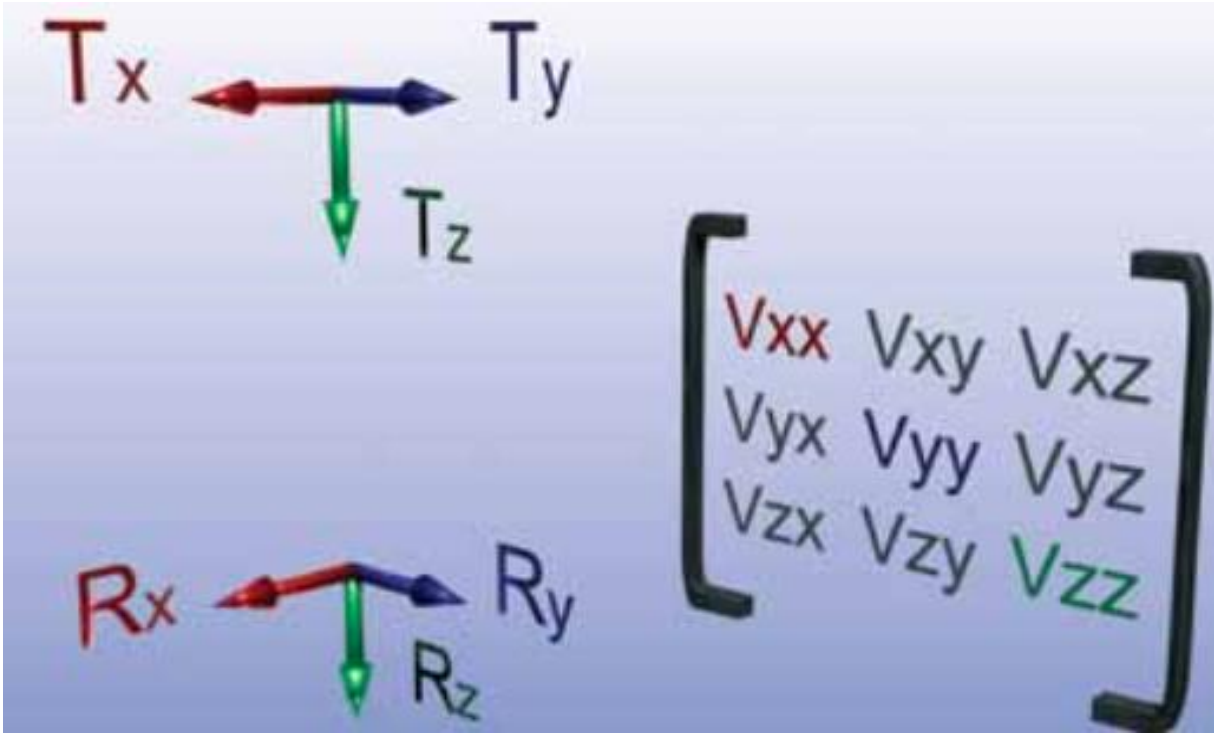

Figure 5 RT scanner tool*:* The collocated transmitter and one receiver (left), and the nine resistivity measurements (right), for x,y and z directions (Schlumberger, 2009).

2.3.2 Resistivity in Anisotropic Reservoirs

The resistivity of stacked layers can be measured either parallel to the layers, or across the layers. The parallel measurement can be described as a parallel circuit. Equation 1 implies that the smallest resistor in a parallel circuit, will have the largest impact on the final resistivity result. This is due to more current flowing through the smaller resistors.

$$R_{total} = \frac{1}{\frac{1}{R_1} + \frac{1}{R_2} + \frac{1}{R_i}} \qquad \text{Equation 1}$$

The vertical measurement across the stacked layers can be described as a series circuit where all resistors present are added together. Equation 2 implies that the largest resistor will have the largest impact on the final resistivity result (Anderson et al., 2008).

$$R_{total} = R_1 + R_2 + R_i \qquad \text{Equation 2}$$

The uniaxial tool has formation currents that flow in horizontal loops, which can be considered as a parallel circuit. Due to this, only the horizontal resistivity (R_h) will be measured, and the lowest resistivity value will dominate the recording. The triaxial tool has currents that flow in both horizontal and vertical loops, and can therefore be considered a parallel circuit as well as a series circuit. From the measurements the series circuit across the layers, the vertical resistivity (R_v) can be obtained.

The difference between the calculated R_v and R_h will be an indicator of the anisotropy in the formation (see example in Figure 6), which again can be an indicator of a thin-bedded clastic sequence in a hydrocarbon filled reservoir. Anderson et al. (2008) states that a separation ratio of 5 or more, should be an indication for thin bed of shale within a sandy formation. An example of this can be observed in well 7220/8-1 and 7220/5-1 (see Figure 6), where the Rv/Rh ratio increases with increasing shale content in the sandy formations and shows indications of laminations due to separation ratio > 5.

The R_v value can be used for further calculations to obtain resistivity of the potential sand layers between the shales. R_{sand} can be calculated using Equation 3 or Equation 4. The shale effects in the volume measured must be removed in order to provide an accurate R_{sand} value. When R_{sand} is calculated, the shale and sand fraction (F_{shale} and F_{sand}) is determined from other logs, such as the gamma ray (GR) log or the Elemental Capture Spectroscopy (ECS) sonde. $R_{shale\text{-}h}$ and $R_{shale\text{-}v}$ are determined from a clean shale formation beyond the laminated section (Anderson et al., 2008).

$$\frac{1}{R_h} = \frac{F_{sand}}{R_{sand}} + \frac{F_{shale}}{R_{shale-h}} \qquad \text{Equation 3}$$

$$R_v = F_{sand} * R_{sand} + F_{shale} * R_{shale-v} \qquad \text{Equation 4}$$

Well 7220/8-1 Well 7220/5-1

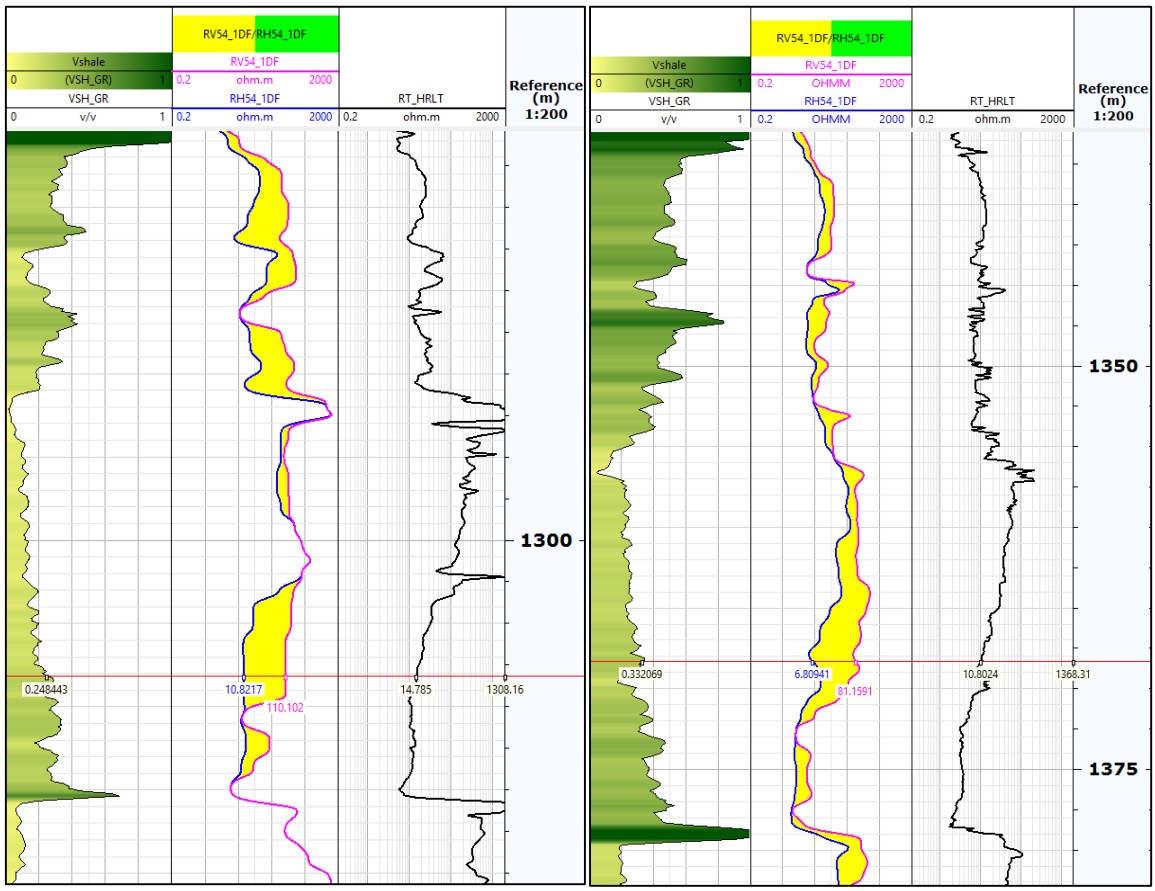

Figure 6 Shale volume (V_{shale}) plotted together with R_v (RV54_1DF), R_h (RH54_1DF) and R_t (RT_HRLT) from well 7220/8-1 and 7220/5-1 Techlog data.

2.4 Nuclear Magnetic Resonance (NMR)

Nuclear magnetic resonance (NMR) is a logging method used for analysis of porosity distribution, fluid type and permeability. These measurements are based on interactions of hydrogen nuclei (protons) with the pore structure and fluid present (Skogen, 2013).

The more common magnetic resonance imaging (MRI) is a measurement conducted on humans from the outside. The NMR is measured by a tool inside the volume of investigation and is therefore referred to as an inside out measurement.

The NMR tool has a magnet that produces a magnetic field. This magnetic field magnetizes the formation materials in a certain direction. The tool also includes an antenna that transmits bursts of radio-frequency energy, as an oscillating magnetic field. Between these precisely timed pulses, the antenna listens for echoes of decaying signals from the hydrogen protons that are in resonance with the permanent magnetic field. The proton resonance frequency forms a linear relationship with the strength of the permanent magnetic field. The volume around the tool can be investigated by tuning of the transmitted and received energy (Coates et al., 1999, pp. 1-32).

Magnetic resonance tools can provide three types of information:

- Quantities of fluid in rock.
- Properties of the fluids.
- Pore size.

The tool is able to directly measure the hydrogen nuclei density of the fluids present in the formation. As the density of hydrogen nucleus in water in known, the measurement can be converted to porosity without any knowledge about the rock matrix. The tool can be run at a certain pulse in order to detect fluids and their properties (Coates et al., 1999).

Both the NMR and neutron tool responses to hydrogen in formations, however the physics of the two tools are rather unlike. Three key differences are described in the book “Practical Petrophysics” written by Kennedy, M. (2015, pp. 130):

1. The NMR tool only responds to hydrogen. This is in contrast to the neutron tool, which more sensitive to other elements as well.

2. The NMR tool has a very precisely defined volume of investigation. Different tools have different shapes but they all have non-diffuse boundaries and any atom outside that barrier cannot contribute to the signal.

3. The NMR tool does not respond to the hydrogen that forms part of a clay molecule. This is again in contrast to the neutron log, which cannot distinguish the environment the hydrogen is in.

2.4.1 NMR Logging Raw Data

Before the NMR tool is activated in the borehole, the nuclei in the formation are randomly oriented. The nuclei are put into motion when the magnetic field (B_0) is generated, and they start to reorientate. The tool's magnet polarizes the spin axes of the nucleus before the antenna is activated and the nucleus are tipped away from their equilibrium position. The field is later removed and the nuclei are tipping back to the original aligned field from the magnet.

The pulse sequences from the antenna are used to generate series of echoes, also called echo trains. These echo trains are referred to as the raw NMR data. The amplitude of the spin echoes is measured as a function of time and is proportional to the quantity of hydrogen nuclei within the measured volume. This measurement can be converted to provide a porosity for the formation (Coates et al., 1999, pp. 1-32).

Several parameters are set for NMR data acquisition in order to provide the best data accuracy. In the book written by Coates et al. (1999) these parameters are described as:

- Inter echo spacing (TE): the time between the individual echoes in an echo train.
- Polarization time (TW): the time between the cessation of measurement of one echo train and the beginning of measurement of the next echo train.

There also exists different properties of the pore fluids that will affect the echo trains. These are described as:

- Hydrogen index (HI): a measure of the hydrogen atoms in the fluid.
- Longitudinal relaxation time (T1): an indication of how fast the tipped protons relax longitudinally (relative to the axis of the static magnetic field).

- Transverse relaxation time (T2): an indication of how fast the tipped protons in the fluid relax transversely (relative to the axis of the magnetic field).
- Diffusivity (D): a measure of the extent to which molecules move at random in the fluid during an acquisition cycle.

By inversion, the decay data from the spin-echoes can be converted to a T2 distribution. The T2 distributions are generated with different depth increments, depending on the tool used. The resolution of the tools will in general vary from 0.5 to 2.0 m (Kennedy, 2015, pp. 129-133).

The T2 distribution can be displayed as a waveform, image or bin plot. This result is the most probable transverse relaxations that produced the echo train and will correlate with pore sizes when the formation is fully water saturated. If other fluids are present, the distribution will be modified due to the type of fluid (Coates et al., 1999, pp. 1-32).

2.4.2 NMR Logging

NMR logging can provide porosity, pore-sizes, bound water and permeability data from its relaxation measurements. These measurements are based on the decay times (T1 and T2) of hydrogen nuclei, caused by magnetic interactions between protons.

T1 is the measurement of a proton system that transfers energy to its surroundings. When the proton relaxes to its low-energy state, energy is emitted before the proton aligns with B_O. T2 come from a dephasing mechanism, where no energy is transferred.

T1 and T2 can be compared in order to detect different stages of the relaxation. For protons in a reservoir fluid with homogeneous static field, the measurements will provide a T2 relaxation approximately similar to T1, while in a gradient field T2 will be smaller than T1. The fluid diffusivity mechanism is mainly controlled by the field gradient and inter-echo spacing. Protons in solids will show a much larger T1 than T2 (Coates et al., 1999, pp. 1-32).

The three main relaxation mechanisms for fluids in pores described by Coates et al. (1999. Pp.45-50) are:

- Bulk relaxation, affecting T1 and T2.
- Surface relaxation, affecting T1 and T2.
- Diffusion relaxation, only affecting T2.

The three relaxation mechanisms have an unequal impact on different fluid types, pore sizes, wettability and strength of surface relaxation. For a water wet rock, brine has got a T2 relaxation that is mainly dominated by the surface relaxation, while in heavy oil the T2 is mostly affected by the bulk relaxation. For light oil, a combination of both bulk and diffusion relaxations affects T2 the most. In gas, T2 is only dominated by diffusion. T2 is in general always faster than, or the same as, T1 (Coates et al., 1999, pp.1-32).

2.4.2.1 Bulk Relaxation

Bulk relaxation is the fluids own relaxation, controlled by physical properties in the fluids composition. This relaxation mechanism can be measured in a lab by filling a container with the particular fluid and expose it to a magnetic field and pulse sequences. This way there will be no surface relaxation interfering with the bulk relaxation, given that the container has a sufficiently large volume. Temperature and pressure is also parameters that can affect this measurement (Coates et al., 1999, pp. 45-51).

2.4.2.2 Surface Relaxation

Surface relaxation occurs at the grain surfaces on the rock, at the interface between fluid and solid. The mechanism is dependent on the ratio between the pore surface and fluid, but also varies with mineralogy for different rock types.

This relaxation mechanism in independent of temperature and pressure. For this reason, NMR measurements on fluids that have a T2 relaxation mainly controlled by surface relaxivity can be conducted in a laboratory and the result can be directly applied in NMR borehole logging (Coates et al., 1999, pp. 45-51).

2.4.2.3 Diffusion-Induced Relaxation

For Gas, light oil, water and some medium-viscosity oils, diffusion-induced relaxation mechanism is an important tool for detection. T2 is increased when molecular diffusion causes dephasing in a gradient magnetic field. The dephasing is caused by molecules moving into an area where the strength of the magnetic field is different, and the precession rate changes.

Physical properties, together with temperature and pressure, affects the diffusion coefficient. The coefficients for water, gas and oil will increase with increasing temperature. With increasing pressure, the diffusion coefficient for gas will decrease due to the increasing density. Diffusion has no impact on the T1 relaxation (Coates et al., 1999, pp. 45-51).

2.4.3 NMR Derived Pore Size and Porosity

Due to the NMR tool's unique sensitivity to relaxation times for hydrogen nucleus, the measurement is independent of rock matrix. Water filled micro porosity will act like a solid when interpreting NMR data, due to a very rapid relaxation time, and leads to an easier way to distinguish between bound and free fluids. The NMR data is also useful when it comes to distinguishing between hydrocarbon viscosities, compared to conventional logs where this is impossible.

Decay rate (T2) vs. amplitude plots provide information about the fluid types present in the volume investigated. The porosity result from the formation is compared to a measurement conducted in water tank, assuming 100% porosity, and results in a ratio between the two. Three factors for accuracy of the raw porosity measurements are described by Coates et al:

- Sufficiently long TW to achieve complete polarization of the hydrogen nuclei (only issue for light HC or gas).
- Sufficiently short TE to record the decays of fluids in micro pores.
- The number of hydrogen nuclei in the fluid being equal to the number in an equivalent volume of water, HI=1 (only issue for light HC or gas).

A high value for T2 will indicate large sized pores (see example in Figure 7), and a small value small sized pore (see example in Figure 8). The area beneath the T2 curves, or the sum of the bins, represents the total porosity. Assuming the three factors above are satisfied, the NMR porosity data will be the most correct compared to porosity data from other logging tools (Coates et al., 1999, pp. 1-32).

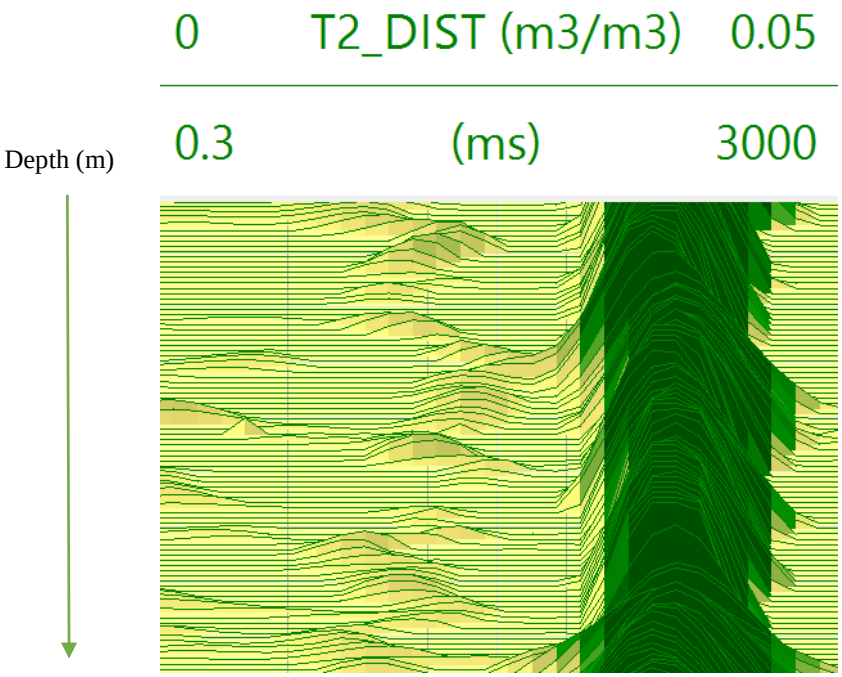

Figure 7 Typical T2 distribution for large sized pores in sandy formations (from well 7220/8-1, Techlog data).

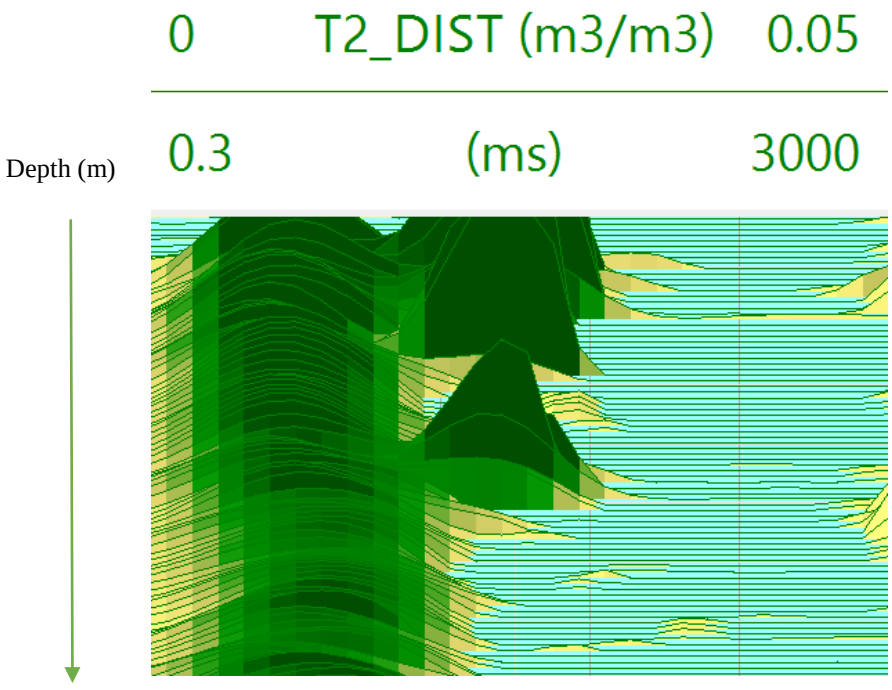

Figure 8 Typical T2 distribution for small sized pores in shale (from well 7220/8-1, Techlog data).

3. Methodology

3.1 Techlog

The Techlog 2014 software from Schlumberger is applied for all methods conducted in this thesis. Techlog is a wellbore-centric petrophysical application composed of a platform and a suit of add-on application modules. The platform comprises tools for loading, visualizing and editing data. The software collects and combine all wellbore data into intuitive application to carry out analyses. It has the ability to integrate both log and core interpretation in one platform, using real-time workflows for well construction. (Schlumberger, 2015a, Schlumberger, 2015c, Schlumberger, 2015b)

In this thesis several modules of the software is applied, in order to obtain all the information needed for the final result of the petrophysical evaluation. A Techlog project was created, and well log data from well 7220/8-1, 7220/7-1 and 7220/5-1 was imported. In order to gather the relevant data needed, a selected set of wireline logs was saved as a harmonized datasets for further use in Techlog calculations and interpretations.

3.2 Conventional Analysis of Well 7220/8-1

A conventional analysis and zonation of the log data for well 7220/8-1 are conducted by calculating shale volume, porosity, water resistivity and water saturation. A simple zonation based on gamma ray (GR), neutron-density (ND) separation and apparent resistivity (R_t) was performed in order to separate the different lithologies and fluids. The measured depth (MD) to total vertical depth (TVD) conversion was neglected due to small maximum inclination of 3.2°, which provided a depth difference of only 1.0 m (NPD, 2016f).

The shale volume was calculated from the clavier GR method in Techlog, where Equation 5 and Equation 6 were applied with the environmentally corrected gamma ray (ECGR) as an input. Cut-offs were set to default values (see Table 1) from interpretation of the GR log in assumed thick shale formations and clean sands.

$$GR_{index} = \frac{GR_{log} - GR_{min}}{GR_{max} - GR_{min}} \qquad \text{Equation 5}$$

$$Vshale = 1.7 - \sqrt{3.38 - (GR_{index} + 0.7\,)^2} \qquad \text{Equation 6}$$

The porosity was calculated by the Techlog density-porosity method, applying Equation 7 with the density log (RHOZ) as an input. The matrix porosities were obtained from core data (see Appendix A.1) and manually set in the parameter tab. For the clean sand and shaly sand zones matrix density was set to 2.64 g/cm^3 and for shale zones matrix density was set to 2.67 g/cm^3. The fluid density was kept default as 1 g/cm^3 for the zones with HC present. For the water zone the fluid density was obtained from Schlumberger Log Interpretation Chart 2009 (see Appendix A.2) and set equal to the mud filtrate density, 1.03, using temperature (GTM) and formation pressure from formation pressure table (see Appendix A.4) as indicators.

$$\varphi_t = \frac{\rho_{matrix} - \rho_{bulk}}{\rho_{matrix} - \rho_{fluid}} \qquad \text{Equation 7}$$

A formation water resistivity (R_w) was obtained by using the R_{wa} method. This method is based on apparent water resistivity and is computed by Equation 8, derived from Archie's equation assuming S_w=1 in the known water zone. For this operation, both the computed porosity (PHIT_D) and the formation resistivity (RT_HRLT) were used as inputs. The parameters a and m, used in the calculation, were set as default values given by the Techlog software (see Table 1). The water resistivity (R_{wa}) was recorded from a depth in the known water zone at 1416.0 m.

$$R_{wa} = R_{t*}\frac{\varphi^m}{a} \qquad \text{Equation 8}$$

The water saturation (S_w) was calculated by using Archie's equation (Equation 9), applying RT_HRLT and PHIT_D as inputs for R_t and φ_t. The parameters a, m and n were set as default (see Table 1), and the water resistivity was set as the recorded value (0.03 ohm-m) from the R_{wa} result.

$$S_w = \left(\frac{a * R_w}{R_t * \varphi_t^m}\right)^{\frac{1}{n}} \qquad \text{Equation 9}$$

A known gas zone is present in the log data, and due to potential porosity error caused by incorrect fluid density, a flushed zone saturation (S_{xo}) was carried out. First, a temperature corrected mud resistivity (RMS) had to be calculated by Equation 10. The formation temperature (GTEM) was used as input. Resistivity parameters and temperatures for mud salinity (MS), mud filtrate (MF) and mud cake (MC) were obtained from field print (see Appendix A.7) and defined in the parameter tab (see Figure 9).

$$RMF = RMFS * \frac{(MFST + 21.5)}{(FTEMP + 21.5)}$$ Equation 10

Well	Zone	Top	Bottom	RMS	MST	MST unit	RMFS	MFST	MFST unit	RMCS	MCST	MCST unit
7220_8-1	Zone_1	1249	1276.5	0.17	23	degC	0.149	23	degC	0.77	23	degC
7220_8-1	Zone_2	1276.5	1312	0.17	23	degC	0.149	23	degC	0.77	23	degC
7220_8-1	Zone_3	1312	1316	0.17	23	degC	0.149	23	degC	0.77	23	degC
7220_8-1	Zone_4	1316	1353.5	0.17	23	degC	0.149	23	degC	0.77	23	degC
7220_8-1	Zone_5	1353.5	1376	0.17	23	degC	0.149	23	degC	0.77	23	degC
7220_8-1	Zone_6	1376	1379	0.17	23	degC	0.149	23	degC	0.77	23	degC
7220_8-1	Zone_7	1379	1390	0.17	23	degC	0.149	23	degC	0.77	23	degC
7220_8-1	Zone_8	1390	1395	0.17	23	degC	0.149	23	degC	0.77	23	degC
7220_8-1	Zone_9	1395	1422	0.17	23	degC	0.149	23	degC	0.77	23	degC

Figure 9 Parameters for RMF calculation from field print.

The RMF, together with PHIT_D and micro resistivity (RXO_HRLT), were used as inputs for the S_{xo} calculation, applying Equation 11. The S_{xo} average value in the gas zone was then used to calculate a new fluid density from Equation 13. In order to obtain gas density, TVD vs. formation pressure was plotted in Excel (see Appendix A.3) from formation pressure table (see Appendix A.4). Points showing low mobility were ruled out, in order to obtain a linear relation between the points. Trend lines were added to the data points, in the known oil, gas and water intervals. The equation for the trend lines showing value of the slope ($75.769=(\Delta P/\Delta Z)^{-1}$) were displayed and Equation 12 was applied to calculate ρ_{gas}. A density result of 0.13 g/cm^3 was obtained from this calculation, and the fluid density from Equation 13 was then calculated to be 0.7 g/ cm^3. A gas corrected (GC) porosity and saturation calculation was carried out by applying Equation 7 and Equation 9, using the new fluid density parameter for the gas zone. These results were saved as PHIT_D_GC and Sw_GC.

$$S_{xo} = \left(\frac{a * RMF}{R_{xo} * \varphi_t^m}\right)^{\frac{1}{n}}$$ Equation 11

$$\rho_{gas} = \frac{\Delta P}{\Delta Z} + \frac{1}{9.81}$$ Equation 12

$$\rho_{fluid} = \rho_{mf} * S_{xo} + \rho_{gas} * (1 - S_{xo})$$ Equation 13

Table 1 Techlog parameter description for eq. 5-13.

Name	Description	Default value	Unit
a	Tortuosity factor.	1	
m	Cementation exponent.	2	
n	Saturation exponent.	2	
R_w	Formation water resistivity	0.03	ohm.m
R_t	Formation resistivity		ohm.m
S_w	Water Saturation		v/v
Φ_t	Porosity		v/v
R_{sh}	Resistivity shale		ohm.m
RMF	Mud filtrate resistivity	0.065	ohm.m
R_{xo}	Flushed zone resistivity		ohm.m
ρ_{mf}	Density mud filtrate		g/cm^3
ρ_{matrix}	Density of rock matrix	2.65	g/cm^3
ρ_{bulk}	Bulk density log reading		g/cm^3
ρ_{fluid}	Bulk density log reading in 100% water	1	g/cm^3
ΔP	Delta formation pressure		bar
ΔZ	Delta total vertical depth		m
GR_{min}	Gamma ray log reading in 100% matrix rock	10	gAPI
GR_{shale}	Gamma ray log reading in 100% shale	100	gAPI
GR_{log}	Gamma ray reading from log		gAPI

The log was then divided into more detailed zones (see Table 2) based on these calculations, neutron-density and R_v-R_h separations. See Appendix A.11 for display of applied log data with zonation for well 7220/8-1.

Table 2 Zone intervals for well 7220/8-1, displaying depth intervals, lithology and formation fluids.

Name	**Depth interval [m]**	**Lithology**	**Fluid present**
Zone 1	1249.5-1276.5	Shale	
Zone 2	1276.5-1312.0	Laminated shale-sand	Gas
Zone 3	1312.0-1316.0	Laminated shale-sand	Oil
Zone 4	1316.0-1353.5	Sand	Oil
Zone 5	1353.5-1376.0	Laminated shale-sand	Oil
Zone 6	1376.0-1379.0	Shale	
Zone 7	1379.0-1390.0	Laminated shale- sand	Oil
Zone 8	1390.0-1395.0	Sand with dispersed shale	Oil
Zone 9	1395.0-1422.0	Shaly sand	Water

3.3 Calculation of Conventional Results for Well 7220/7-1 and 7220/5-1, and Well Correlations

A basic analysis, similar to the previous, was performed on well 7220/7-1 and 7220/5-1. The MD to TVD conversion was also neglected for these wells due to small maximum inclinations of 4.46° for well 7220/5-1 and 6.0° for well 7220/7-1. This provided a MD-TVD depth difference of 1.0 meter for well 7220/7-1 (NPD, 2016e) and 0.0 m for 7220/5-1 (NPD, 2016d).

Values for water resistivity, matrix densities and fluids are assumed the same as for well 7220/8-1, as the wells come from the same area and penetrate through the same formations. Shale minimum and maximum cut-offs for both well 7220/7-1 and 7220/5-1 are set to 20 gAPI and 130 gAPI, due to interpretations of layers considered as clean sand and shale in both wells.

NPD information (OWC, OGC etc.), shale volume, ND separations, conventional and triaxial resistivities, porosities and saturations from well 7220/7-1 and 7220/5-1 were compared to the similar data from well 7220/8-1, and an interpretation was conducted based on this information.

3.4 Resistivity Calculation Method for Coarse Grained Layers, Applying T2 Distributions and Triaxial Resistivities

In the paper written by Shray and Borbas (2001), two methods for better hydrocarbon estimation of laminated low pay reservoirs are presented. Both methods are based on improvement of resistivity results in coarse-grained layers (in this case, clean sand and shaly sand). The first method is based on the equations described in Chapter 2.3.2, for calculation of R_{sand}. An example for application of these equations in well 7220/8-1 can be obtained from the project thesis written by Olsen, S. G. (2015). This project applies the triaxial resistivities in order to obtain an improved resistivity result for the sand laminas in the laminated sand-shale sections of the reservoir (Olsen, 2015).

The second method describes an approach that combines NMR and triaxial resistivity measurements. This method is applied for well 7220/8-1 in this thesis, due to low resistivity pay zones with resistivity anisotropy present within the reservoir interval (see examples in Figure 10). This method will in theory provide a similar result to R_{sand}, although the shale volume is replaced with volume fractions from T2 distributions.

The T2 distribution is used to calculate the volume fraction of the fine-grained (f_{Vfg}) and the coarse-grained (f_{Vcg}) layer. T2 cut-offs are set to standard values for bound fluids, 0.3 ms and 33 ms. Pre-defined cut-offs for the CMR log are saved in the dataset, and a free fluid porosity log (CMFF) is present. The T2 parameter summarized over time in Equation 14 and can therefore be expressed as total porosity (TCMR) minus the CMFF log. Φ_t was set as TCMR, and the volume fraction for the coarse-grained layer was calculated from Equation 15 (Shray and Borbas, 2001).

$$f_{Vfg} = \frac{\sum_{0.3ms}^{33ms} T_2}{\phi_t} \qquad \text{Equation 14}$$

$$f_{Vcg} + f_{Vfg} = 1 \qquad \text{Equation 15}$$

The volume fractions calculated from Equation 14 and Equation 15 were included in Equation 16, together with R_v and R_h, and a new resistivity for the fine-grained layer was calculated. The "minus solution" for the second term in Equation 16 was applied due to the assumption that $R_{cg} > R_{fg}$ throughout the reservoir. This result was then applied to Equation 17 for calculation of a new resistivity for the coarse-grained layers.

$$R_{fg} = \frac{R_v + (1 - 2 * f_{Vcg}) * R_h}{2 * f_{Vfg}} \pm \sqrt{\left(\frac{R_v + (1 - 2 * f_{Vcg}) * R_h}{2 * f_{Vfg}}\right)^2 - R_v R_h} \qquad \text{Equation 16}$$

$$R_{cg} = \frac{R_v - (1 - f_{Vcg}) * R_{fg}}{f_{Vcg}} \qquad \text{Equation 17}$$

All equations for this method is provided from the paper written by Shray and Borbas (2001). See Table 3 for parameter descriptions.

Table 3 Parameter descriptions for equation 14.-17.

Parameter name	Description	Unit
$\mathbf{R_{cg}}$	Resisitivity coarse grained layer	Ohm-m
$\mathbf{R_{fg}}$	Resisitivity fine grained layer	Ohm-m
$\mathbf{f_{vcg}}$	Volume fraction coarse grained layers	v/v
$\mathbf{f_{vfg}}$	Volume fraction coarse grained layers	v/v

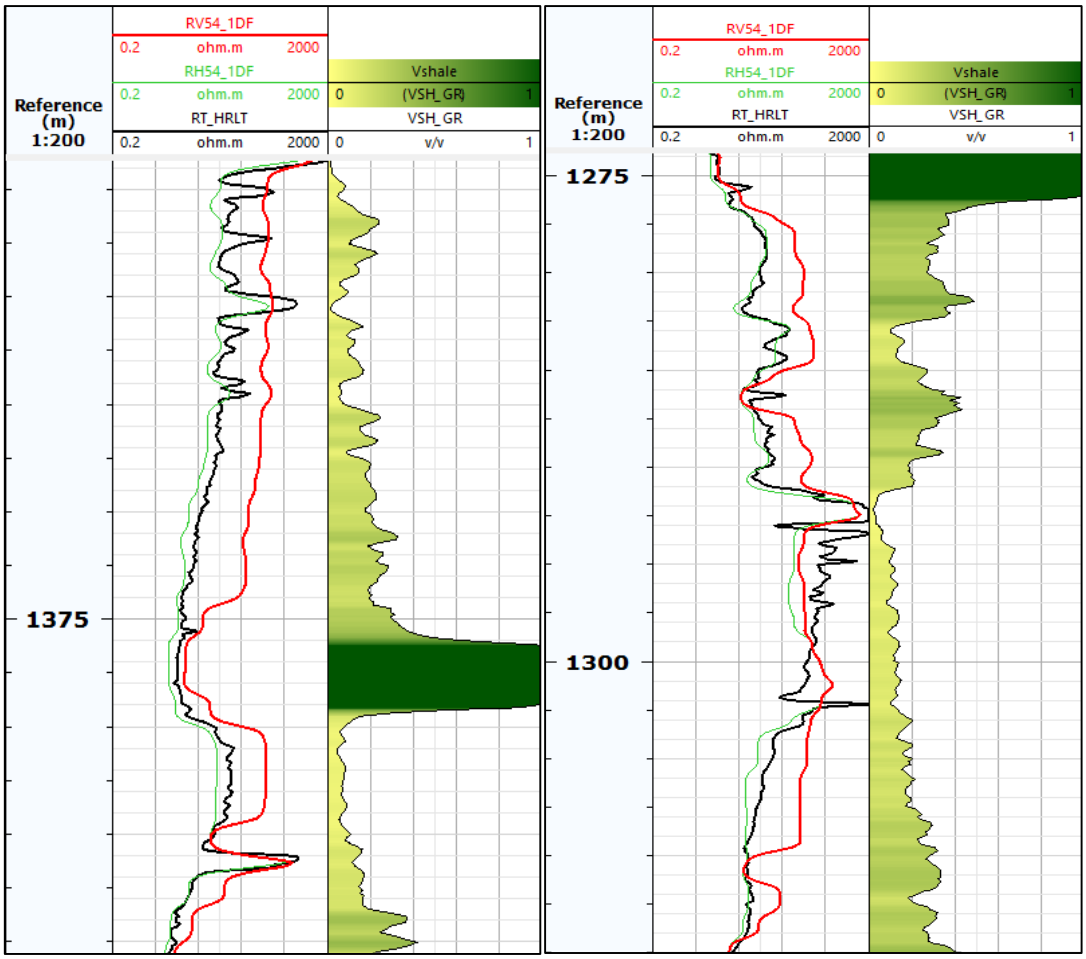

Figure 10 Resistivity anisotropy examples within the reservoir section for well 7220/8-1, displaying separations between the vertival resistivity (RV54_1DF) and the horizontal resistivities (RH54_1F and RT_HRLT). The separation increases with increasing shale volume (Vshale).

3.5 The Density-Magnetic Resonance Method

The Density Magnetic Resonance (DMR) method combines porosity from both density and NMR logs in order to provide a better estimate of total porosity, especially for gas bearing zones. This method is based on the gas equations developed by Freedman in 1977.

When logging a gas bearing zone with a density tool, the response from the measurements might be overestimated because the formation bulk density is reduced. The NMR tool will in the same situation provide an underestimated measurement due to low hydrogen index and inaccurate polarization of the gas. The polarization issue occurs due to the reservoir gas' large longitudinal relaxation time ($T_{1,g}$). To fully polarize the gas, wait times of up to 10 seconds is needed, which is not applicable for routine logging times.

Due to the different reading from the two tools, the porosities will show a separation in the gas bearing zones, which again will be an indication of the gas saturation close to the wellbore. This effect can be compared to the crossover from neutron and density logs when gas present in the formation, but will provide a more reliable result. Because the NMR tool only responses to fluid in the formation, shale and thermal neutron absorbers will not affect the DMR-density crossover as it does to the neutron-density (ND) crossover (Freedman et al., 1998).

In the paper written by Freedman, R., et al., the equations for porosity calculations combining both NMR (TCMR) and density (PHIT_D) derived porosities are described. As the PHIT_D and TCMR logs displayed clear separation within the gas zone in well 7220/8-1 (see Figure 11), this method was carried out in order to avoid applying fluid corrections, as performed in Chapter 3.2. The porosity derived from the equations below is assumed to provide an improved porosity estimate for the gas bearing formation in zone 2.

The DMR porosity (Equation 22) is derived from the response equations for the formation bulk density (Equation 18) and total NMR porosity (Equation 19):

$$\rho_b = \rho_{ma} * (1 - \varphi) + \rho_f * \varphi * \left(1 - S_{g,xo}\right) + \rho_g * \varphi * S_{g,xo} \qquad \text{Equation 18}$$

$$TCMR = \varphi * S_{g,xo} * (HI)_g * P_g + \varphi * \left(1 - S_{g,xo}\right) * (HI)_f \qquad \text{Equation 19}$$

A new parameter, λ, is added to simplify the equation (see Equation 20). This parameter is proportional to the density difference between the gas and liquid phases and is responsible for the gas effect on the density porosity log. Density of fluid phase in the flushed zone is found to be 1.1 g/cm^3 from Schlumberger charts (see Appendix A.5 and A.6), by using the known formation salinity and formation temperature. The matrix density is set to 2.64 g/cm^3.

$$\lambda = \frac{\rho_f - \rho_g}{\rho_{ma} - \rho_f} \qquad \text{Equation 20}$$

Equation 21 provides the density derived porosity

$$PHIT\_D = \frac{\rho_{fb} - \rho_{ma}}{\rho_f - \rho_{ma}} \qquad \text{Equation 21}$$

The gas corrected DMR total porosity is defined in Equation 22. This equation is applicable when there exists gas or light HCs, and the PHIT_D is larger than TCMR. P_g is calculated from the wait time (w) found from CMR report in Appendix A.8, and the T_{1g} which is found from the Schlumberger chart in Appendix A.9, using reservoir pressure as indication. The CMR report states that the hydrogen nucleus are fully polarized, and the wait time is therefore set to infinity. The HI_g is also found from Schlumberger chart (see Appendix A.10), by using the gas density, while HI_f is set to 1 due to water based mud used in the well.

$$\phi = \frac{DPHI * \left(1 - \frac{(HI)_g * P_g}{(HI)_f}\right) + \left(\frac{\lambda * TCMR}{(HI)_f}\right)}{\left(1 - \frac{(HI)_g * P_g}{(HI)_f}\right) + \lambda} \qquad \text{Equation 22}$$

A new, final water saturation was then calculated (S_{W_fin}) using the DMR porosity and R_{cg} resistivity as inputs.

All equations in this chapter is provided from the paper written by Freeman et al. (1998). See Table 4 for parameter descriptions.

Table 4 Parameter description for equation 18.-22.

Parameter name	Description	Unit
ρ_b	Measured formation bulk density	g/cm^3
ρ_{ma}	Formation matrix density	g/cm^3
ρ_f	Density of fluid phase in the flushed zone at reservoir conditions	g/cm^3
ρ_g	Density of gas at reservoir conditions	g/cm^3
φ	Total NMR formation porosity (TCMR)	v/v
HI_g	Hydrogen index of gas at reservoir conditions	
HI_f	Hydrogen index of liquid phase in the flushed zone at reservoir conditions	
$S_{g,sxo}$	Flushed-zone gas saturation	v/v
P_g	Gas polarization function = 1- exp (-W/$T_{1,g}$)	
W	Wait time for CMPG pulse sequence	s
$T_{1,g}$	Gas longitudinal relaxation time at reservoir conditions	s

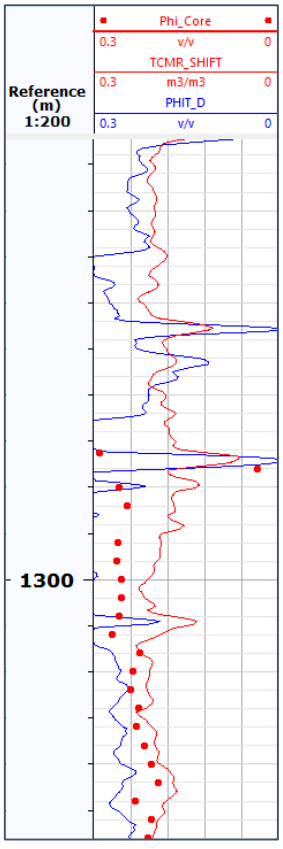

Figure 11 Density (PHIT_D) – NMR (TCMR) porsosity separation in the gas zone for well 7220/8-1, displaying core porsosity (Phi_Core) as a reference.

3.6 Creation of Thomas-Stieber Diagrams for Well 7220/8-1

Shale in a formation can, as mentioned in Chapter 2.2, be distributed in three different ways; laminated, structural and dispersed. The gamma ray response, which is often used to estimate shale volume, can vary with the distribution and geometry of the shales. Thomas and Stieber developed a diagram in order to detect the distribution and the proportion of shales within a sandy formation, by cross plotting gamma ray vs. porosity. For this model it is assumed that shale is the primary destroyer of sand porosity, and the gamma ray is therefore expected to correlate with porosity. On the other hand, gamma ray will not respond in the same way if the shales are distributed as good sorted or by mineralization (Thomas and Stieber, 1975).

In the paper written by Thomas and Stieber (1975, pp. 2), five main assumptions for the model are described:

1. There are only two rock types, a high porosity "clean" sand and a low porosity "pure" shale. The observed in situ porosities are generated by mixing the two.

2. Within the interval investigated, there is no change in shale type and the shale mixed in the sand is mineralogically the same as the "pure" shale sections above and below the sand.

3. The gamma ray responds to the number of radioactive events in a material and thus its mass. The shale fractions we wish to determine are a function of volume. We assume for the Tertiary basins that both sands and shales have comparable grain densities, thus, the radioactivity will be proportional to volume.

4. Constant background radiation will be assumed to be present in all measurements.

5. Counting yields will not change, as rock types are intermixed.

The diagram is constructed so that the GR values are displayed along the x-axis while the y-axis display the porosity values. Porosity and GR endpoints, for both sand and shale are set from clean formations, and an endpoint for dispersed shale are calculated by multiplying the two ($\phi_{sand} * \phi_{shale}$). Between these endpoints, lines are drawn forming a triangle. These lines are indicators of fractions of clean sand, shale laminas and dispersed shale (see Figure 12). Structural shale is assumed to plot in the upper section of the diagram, above the laminated shale line. Depending on the porosity and GR values for each depth point in the well, a structure of points will form in the cross plot and an interpretation for the different shale distributions can be performed (Thomas and Stieber, 1975).

The Thomas-Stieber (TS) method is applied to the dataset for well 7220/8-1 in order to plot the laminated from the possible dispersed shales and compare the result with the zonation based on conventional analysis. Techlog has a built in function for creation of the diagram. PHIT_D_GC, DMR and ECGR are used as inputs and parameters for endpoints are set manually and modified, based on the distribution of the points plotted (see Table 5).

As the points plot down along the right line, from the clean sand to the dispersed endpoint, the more dispersed shale is present (see Figure 8). Points that plot along the upper line, will indicate different amount of laminations from the clean sand towards 100% laminated shale (Thomas and Stieber, 1975). As described by Kennedy, M. (2015, pp. 348), "Any point within the triangle defined by these end points consists of laminated shale and shaly sand. The relative amounts are found by a geometric construction." Lines can thus be drawn in order to see the percentage of each distribution, as in Figure 12. In this case, the diagram is only used for quality check of the pre made zones of shaly and clean sand.

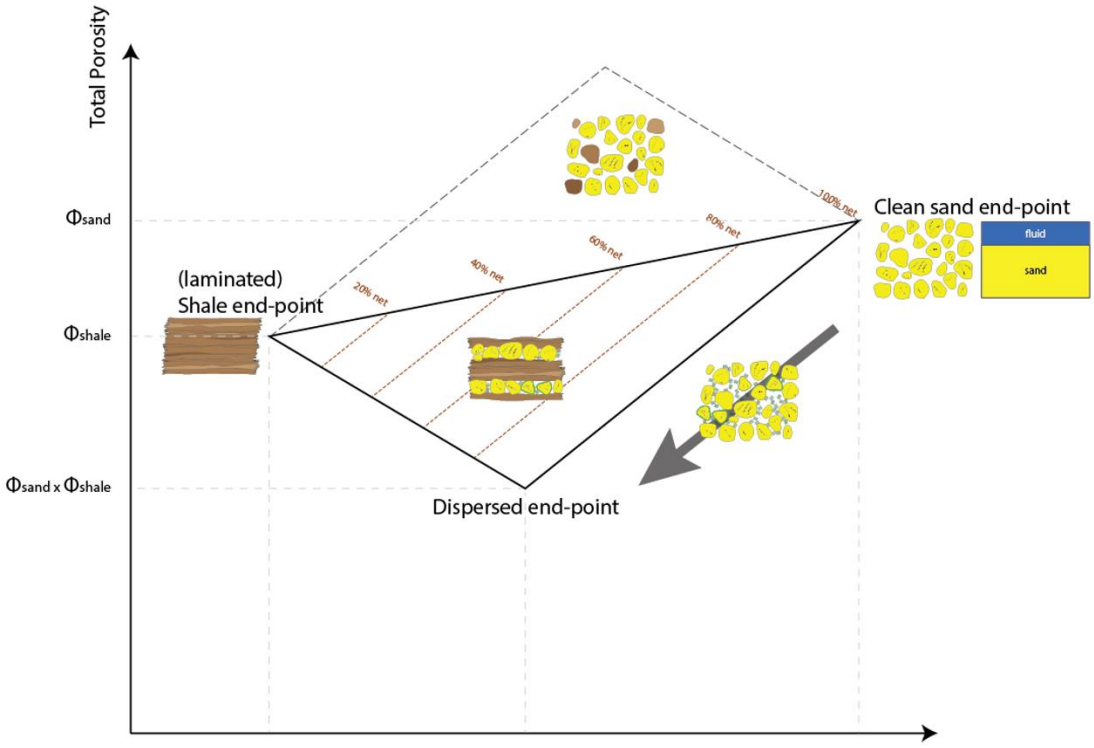

Figure 12 Thomas-Stieber diagram example, displaying endpoints for shale, clean sand and dispersed shale (Brandsen, 2016).

Table 5 Thomas-Stieber input parameters for creation of Gamma ray-Porosity cross plot

Parameters	Value (DMR input)	Value (PHIT_D input)	Unit
Clean sand GR	10	11	gAPI
Shale GR	125	127	gAPI
Clean sand porosity	0.29	0.29	v/v
Shale porosity	0.12	0.11	v/v
Shale resistivity	3	3	ohm.m
Formation water resistivity	0.03	0.03	ohm.m

3.7 Techlog Summary Calculation and Merging of Shale Volume, Porosity and Bulk Fluid Results

As a final calculation, a Techlog summary was conducted to the results from the previous chapters. This summation was performed using Sw_AR_fin, and provided results for the clean depth intervals (ROCK), reservoir intervals (RES) and hydrocarbon impregnated reservoir intervals (PAY).

For this thesis, the hydrocarbon pore thickness (HCPOR-TH) in the PAY intervals were the result wanted in order to summarize all the hydrocarbons present. Cut-off values for porosity, water saturation and shale volume were set in order to limit the calculations to the good quality reservoir rock (see Table 6).

Techlog applies Equation 23 for calculation of HCPOR-TH in every zone. In this equation, the porosity and Sw_AR_fin are averaged values (Av_Porosity, Av_Water Saturation) for each zone interval and the net thickness is defined by the cut-off values. The result was saved in a summary table under the result tab in the workflow window.

$$HCPOR - TH = net * \varphi * (1 - S_w) \qquad \text{Equation 23}$$

Table 6 Cut-off values for summaries.

	Shale Volume	**Porosity**	**Water saturation**
Max	0.5	0.6	0.6
Min	0	0.1	0

The HCPOR-TH PAY result in the shale-sand intervals were multiplied by the laminated sand fraction, V_{sand} (1-V_{sh}), to obtain a better estimation of the HCs present. In the clean sand, the laminated shale fraction was considered as 0, thus V_{sand} were set to 1.

The final step in this thesis was to merge the results for bulk fluid volume (BVW) from Archie water saturation calculation, using both DMR and R_{cg} as inputs (BVW_AR_fin), shale volume and DMR porosity in order to observe the distribution of shale, sand, hydrocarbons and water. Different colours were applied to the separations between the logs in order to present the fraction of each element.

4. Results

The content presented in this chapter provides the main results for the methods conducted in Chapter 3. These results are based on log data for well 7220/8-1, 7220/7-1 and 7220/5-1. Data for all wells are displayed together with result for the conventional analyses in Appendix A.12-A.14.

4.1 Well Correlations

Conventional log data and results for well 7220/8-1 were compared to the similar data in well 7220/7-1 and 7220/5-1. The three wells were marked with indicators for Top Stø formation, Top Nordmela Formation, OGC and OWC (see Figure 14, next page). The interpretation was conducted in between these markers, in order to observe similarities between the same formations in each well. The interpretation is discussed further in Chapter 5.

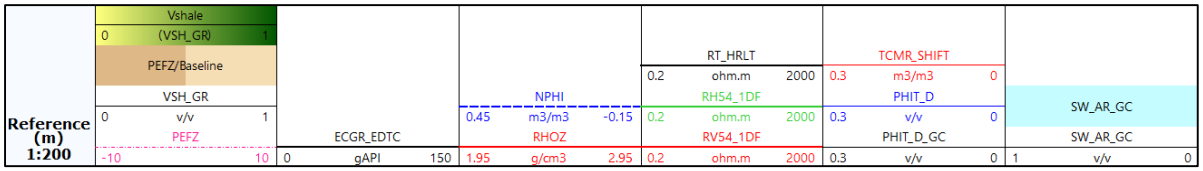

Figure 13 Logs names with colours for correlation result in Figure 14 (from left to right for all three wells).

7220/8-1 7220/5-1 7220/7-1

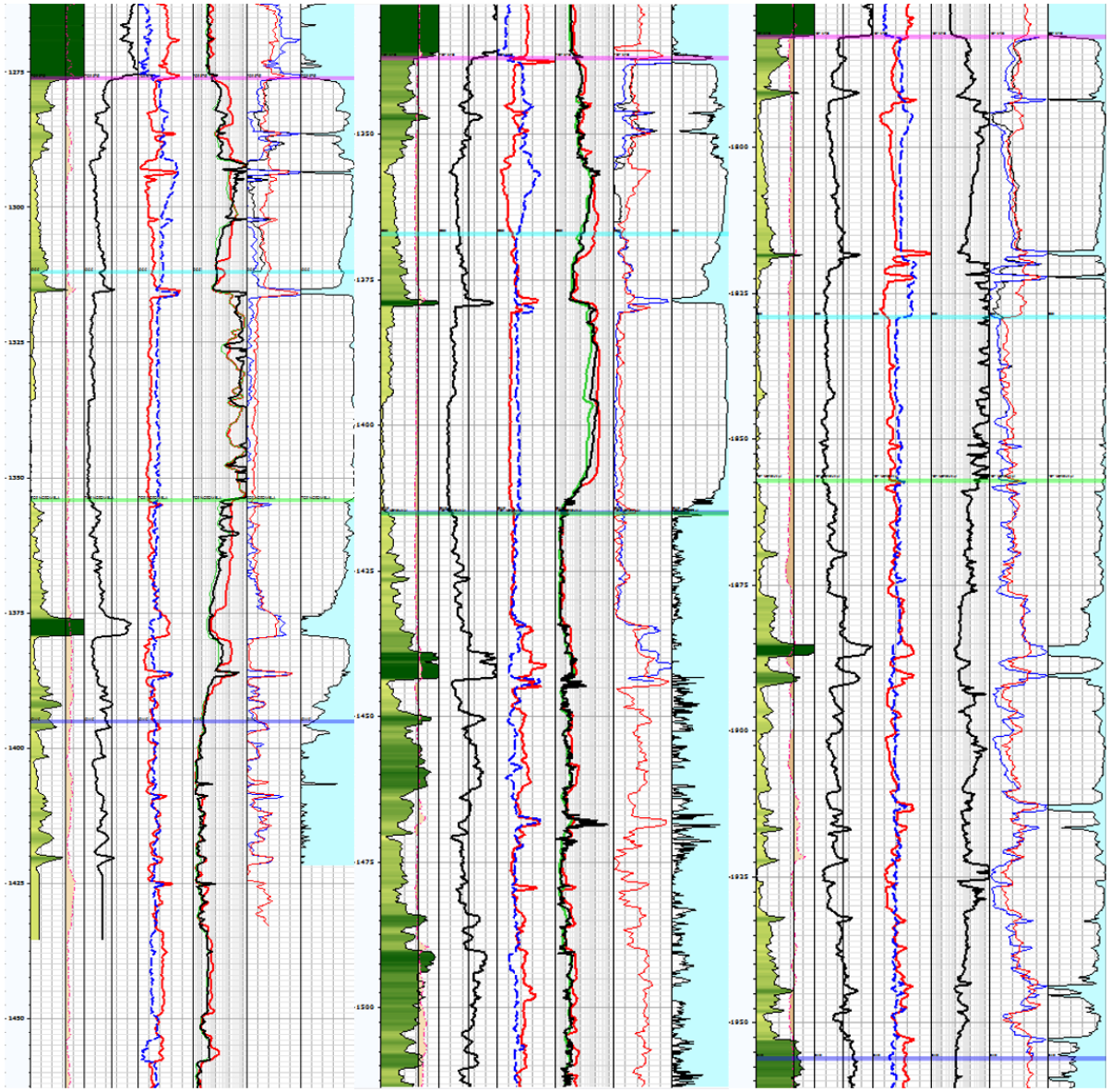

Figure 14 Log data and conventional analysis results for well 7200/8-1, 7220/5-1 and 7220/7-1 for comparison. Techlog markers are set for Top Stø (pink), OGC (turquoise), OWC (blue) and Top Nordmela (green). See Figure 13 for log names with colours.

4.2 R_{cg} Resistivity Result

The calculated R_{cg} resistivity for well 7220/8-1 is presented in Appendix A.15. The resistivity log shows a good correlation with R_v in the laminated hydrocarbon filled zones (see example in Figure 15).

The resistivity result for zone 4 is to some extent modified in excel, due to negative solutions under square root for the second term in Equation 16, which lead to no solution for some intervals within the clean sand. The new solution is saved as Rcg_minus_corr.

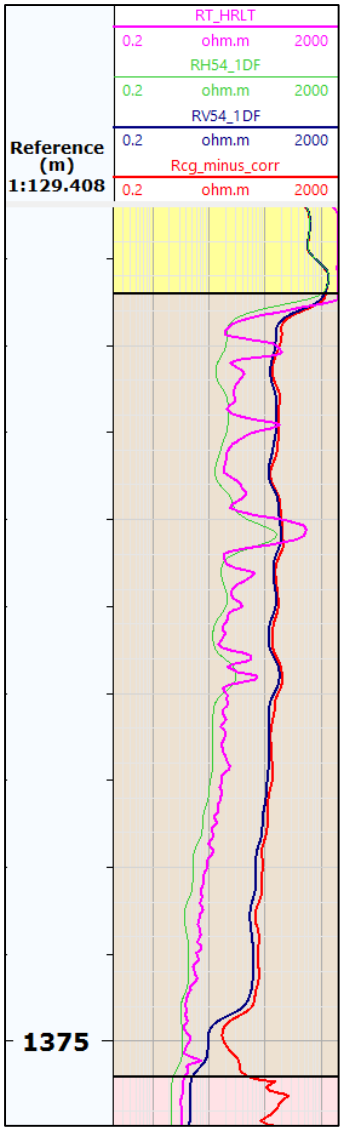

Figure 15 Example from well 7220/8-1 resistivity differences between R_{cg}, R_v (RV54_1DF) and the horizontal resistivities R_h (RH54_1F and R_t (RT_HRLT) in laminated shaly-sand zone 5 (1353.5 m – 1376.0 m).

4.3 DMR Porosity Result

The calculated DMR porosity for well 7220/8-1 is presented together with both density (PHIT_D), NMR (TCMR_SHIFT) and core (Phi_Core) porosities in Appendix A.15. DMR shows good correlation with core porosity throughout the log. TCMR and PHIT_D also shows separation within the gas zone, as seen in Figure 16.

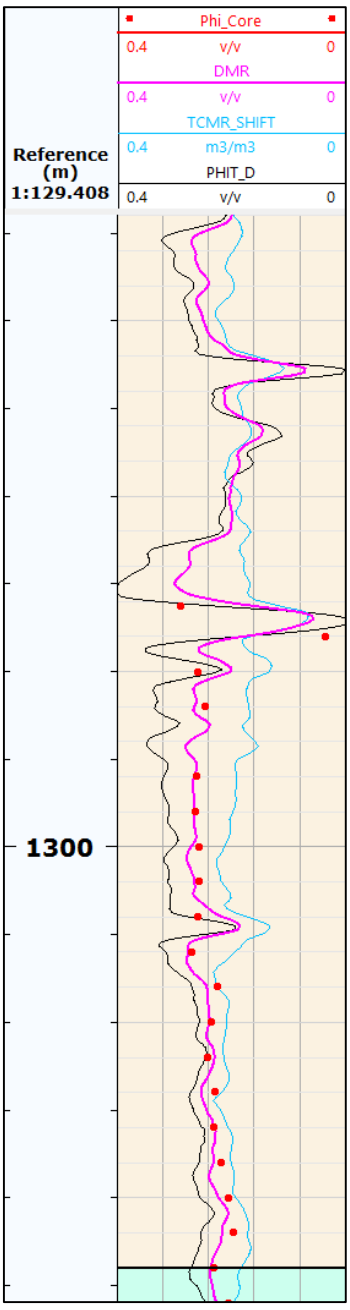

Figure 16 DMR vs. depth shifted TCMR porosity (TCMR_SHIFT), density porosity (PHIT_D) and core porosities (Phi_Core) in gas zone 2 (1276.5 m – 1312.0 m).

4.4 Thomas-Stieber Diagrams

Two Thomas-Stieber diagrams created for DMR and gas corrected density porosity, are presented for well 7220/8-1 in

Figure *17* and Figure 18. The points plotted on the diagrams show different colours as indication for each zone. Both diagrams indicates that zonation of the laminated shaly sand and the clean zones are correct.

The same scale is used for both cross plots, but endpoints are modified to some extent, based on the point distribution fit (see Table 5). The plot applying DMR as porosity input displays a slightly closer gathering of point along the laminated line, than the plot applying PHIT_D_GC.

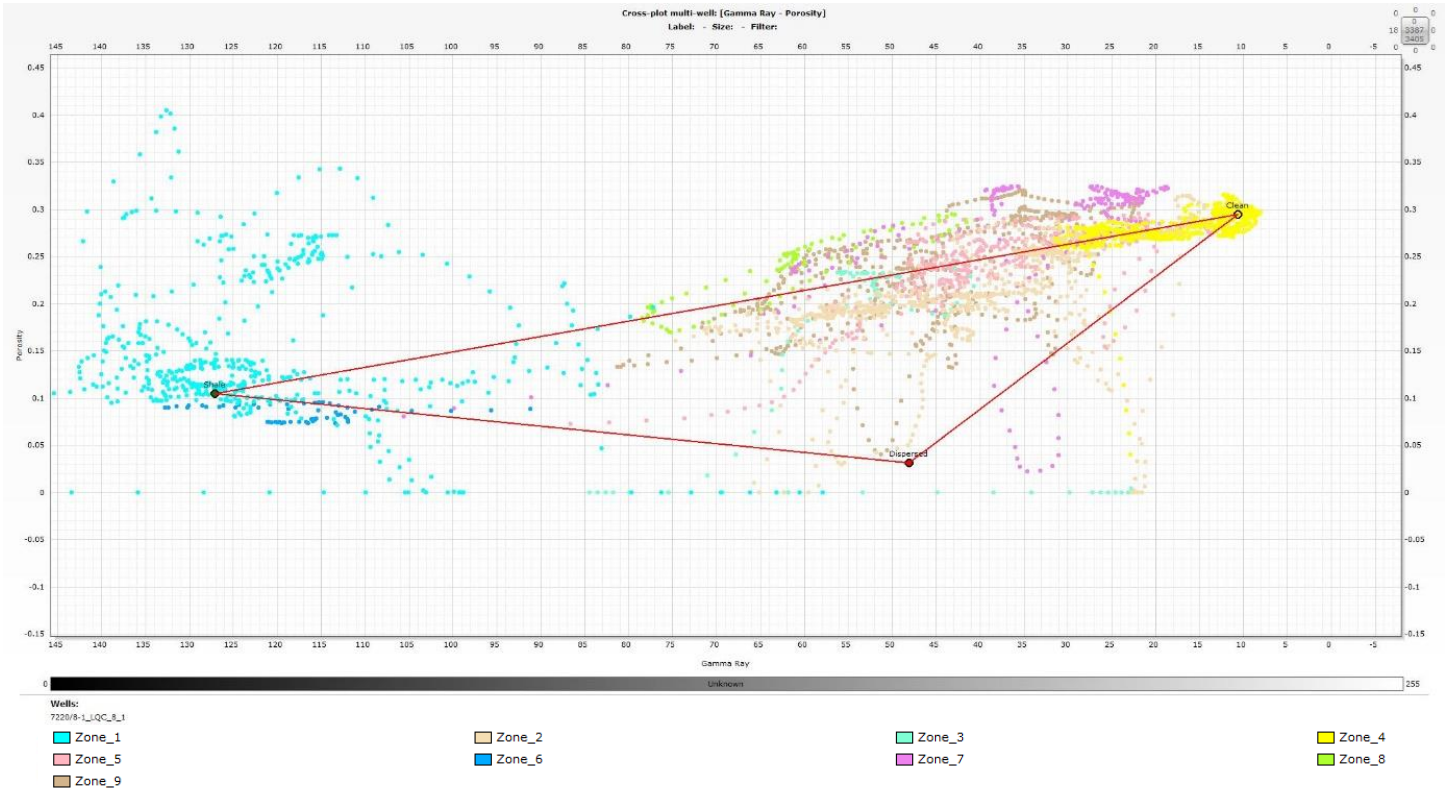

Figure 17 Thomas-Stieber diagram for well 7220/8-1 using ECGR and PHIT_D_GC as inputs.

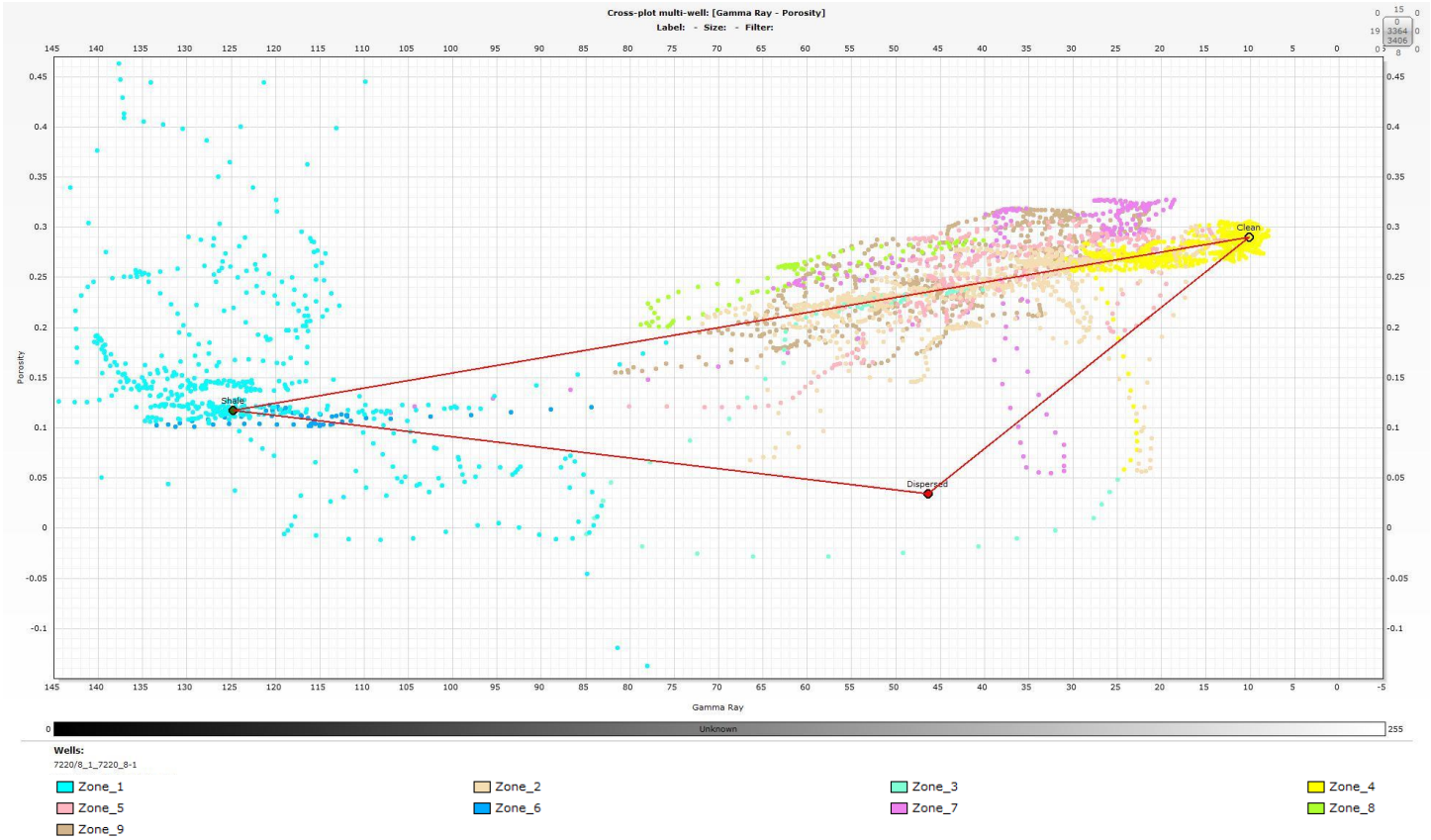

Figure 18 Thomas-Stieber diagram for well 7220/8-1 using ECGR and DMR as inputs.

4.5 Techlog Summary and Log Merging Result

Table 7 displays the Techlog summary results for well 7220/8-1. These results were obtained using the final Archie water saturation (S_{w_fin}), DMR and V_{sh} as inputs. The table sums up the pay results for the hydrocarbon pore thicknesses for each zone and multiplies it by 1 minus the averaged shale volume (= Av_Sand_Volume) for each zone, as its main result. This table presents a total hydrocarbon pore thickness of 22.8 m in the reservoir section of 120.0 m.

The display of the merged results for porosity, shale and bulk fluid volume in Figure 19 illustrates different colours representing fractions of lithologies and fluids in the formations. The shale volume is represented on the left with a dark green colour and the yellow colour represents the sand matrix. The DMR porosity curve delineates the fluid fractions in the pores, where the hydrocarbon saturation are plotted with a bright green colour and the blue represents the water saturation.

Table 7 Summary result from Techlog workflow displaying depth (top and bottom), hydrocarbon pore thickness (HCPOR_TH), average sand and shale volume, porosity and water saturation for each zone in well 7220/8-1.

	Workflow Table Result MD								
Lithology	**Zone**	**Top (m)**	**Bottom (m)**	**HCPOR-TH (m)**	**Av_Sand Volume**	**Av_Shale Volume**	**Av_Porosity**	**Av_Water Saturation**	**HCPOR-TH (m) * Av_Sand Volume**
Shale	1	1249	1276.5		0	1			0
Shaly sand	2	1276.5	1312	7.377	0.79	0.21	0.233	0.085	5.82783
Shaly sand	3	1312	1316	0.531	0.717	0.283	0.223	0.206	0.380727
Sand	4	1316	1353.5	9.816	1	0	0.277	0.046	9.816
Shaly sand	5	1353.5	1376	5.279	0.836	0.164	0.255	0.077	4.413244
Shale	6	1376	1379		0	1			0
Shaly sand	7	1379	1390	2.564	0.863	0.137	0.287	0.126	2.212732
Shaly sand	8	1390	1395	0.205	0.7	0.3	0.26	0.422	0.1435
Sand (Shaly)	9	1395	1422	0.031	1	0	0.298	0.585	0.031
Total HC (m)									22.825033
Total gas (m)									5.82783
Total oil (m)									16.997203

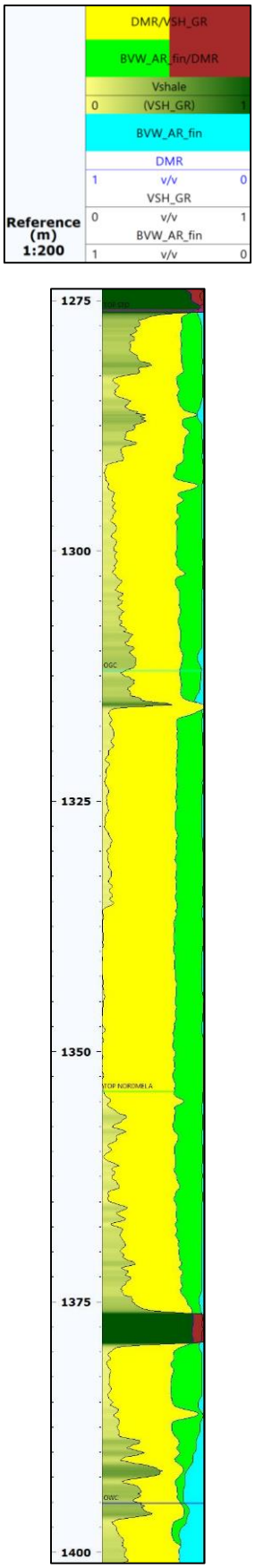

Figure 19 Bulk fluid volume (BVW) vs. DMR and shale volume (V_{sh}), displaying the fraction of shale (dark green), sand matrix (yellow), hydrocarbons (bright green) and water (blue) in in well 7220/8-1. The figure also include fluid contact and formation markers.

5. Discussion and Further Work

5.1 Discussion of Results

The results from the well correlation (see Figure 14) shows good connections between all wells. Formation tops for Stø and Nordmela (see Appendix A.16), OGC and OWC from NPD are used as a base for the interpretation of the wells. The OGCs and OWCs defines the reservoirs to exist within two formations, Stø and Nordmela, for well 7220/8-1 and 7220/7-1, and only in the Stø formation for well 7220/5-1. In well 7220/7-1 the reservoir is located at a greater depth than in well 7220/8-1 and 7220/5-1, where the reservoirs are at quite similar depth intervals. The reservoir intervals range from 175.0 m in well 7220/7-1 to 120.0 m in well 7220/8-1 and 75.0 m in well 7220/5-1.

The shale volumes show more or less the same trends for all wells. In well 7220/5-1 a small increase for the shale volume in the upper half section of the reservoir, can be observed. No other indications, such as ND separation decrease or Rv-Rh increase, were seen, and due to this it is assumed that a small error in the premade cut-offs could be the reason for the dissimilarity.

Above the Top Stø marker a thick cap rock shale can be observed in both 7220/7-1 and 7220/5-1, as in 7220/8-1. Under this marker and down to the GOC, the ND separation increases due to decreased shaliness for all wells. A more shaly interval of approximately 1.0 m can be observed right beneath the OGC in well 7220/8-1 and 7220/5-1, and right above in well 7220/7-1. In well 7220/8-1, a clean sand zone can be observed from this shale and down to Top Nordmela, with low shale volume, constant ND separation and high resistivities. The same trends can be seen in well 7220/5-1 and 7220/7-1. The triaxial resistivities shows a R_v/R_h separation ratio up to 6 in this zone for well 7220/5-1, while the PEF log shows a log value of under 3 b/e. As stated in Chapter 2.3.2, a R_v/R_h ratio of 5 or more would indicate thin-bedded laminations of shale within the sand. In well 7220/8-1 this cut-off is interpreted to be even lower, and is set to be approximately 3. In order for this to be true the PEF log would be expected to show larger values than it does, and together with the shale volume results, the R_v-R_h separation is neglected as an indication for shaly sand and proceeded as a clean interval.

The apparent resistivity (R_t) show similar trends throughout the reservoirs in all wells, with increasing values for clean sand zones and decreasing values with increasing shale volumes. Only apparent resistivity can be obtained for well 7220/7-1, and a correlation regarding

anisotropy cannot be conducted for this well. The R_v-R_h separation in the two other wells seems to correlate well with increasing shale volume, which indicates that most of the shale present is distributed as laminated. One exception is found below the OWC in well 7220/5-1, where the shale volume significantly increases and at the same time a decrease in the R_v-R_h separation can be observed. This could be an indication of a dispersed shale zone. In well 7220/8-1 a similar interval of approximately 1.0 m can be observed right above the OGC. This zone is neglected as a dispersed zone for the summary calculation, due to narrow interval height.

The R_v-R_h separations for well 7220/8-1 and 7220/5-1 shows similarities throughout the reservoir sections. The separation is large both wells in the gas zone. For well 7220/8-1 the separation can be seen up to Top Stø, and in 7220/5-1 the separation is at its largest around the OGC. The strongest R_v-R_h separation for well 7220/8-1 can be observed in shaly-sand Zone 5, within the Nordmela formation. The same laminated zone cannot be interpreted from triaxial resistivities in well 7220/5-1, due to Nordmela FM existing below the OWC.

The gas corrected density porosity logs shows similar values throughout the reservoir sections for all wells, showing a small decrease with increasing shale volume. The porosities for the clean sand zone interval in well 7220/7-1 shows a slightly lower average value compared to the two other wells, which have a consistent porosity of approximately 0.28 - 0.30 v/v. This difference might be due to compaction from overburden, as the reservoir found in this well is located at a much greater depth than in the two other wells. The corrected water saturation also seems to provide a similar result for all wells, with a low saturation in the clean sand intervals (< 0.1) and increased values with increasing shaliness.

The fluid contacts are modified for both well 7220/5-1 and 7220/7-1 due to interpretation of both ND separation, TCMR - PHIT_D separation and resistivity changes. For well 7220/5-1 the OWC is moved two meters down, to 1367.0 m, due to TCMR-PHIT_D and ND separation decrease. The OWC is moved down one meter, to the Top Nordmela marker at 1415.0 m, due to resistivity and ND separation decrease. For well 7220/7-1 the OGC is moved down one meter, to 1829.0 m, also due to TCMR-PHIT_D and ND separation. No lithology changes were observed around the contacts, and the ND-separation is therefore considered to be controlled by the fluids present, and not due to decreasing/increasing shaliness.

The Thomas-Stieber (TS) diagrams in Figure 17 and Figure 18 provides an orderly pictures of the distributions of shale in each zone for well 7220/8-1. The diagram using DMR as porosity input shows a slightly closer gathering of points around the laminated line for the laminated sand-shale zones, and at the same time clear indications for the clean zones. This dissimilarity could be due to small differences in the porosity calculations and the endpoints set for the two different plots. Remarkable trends on both diagrams indicates wrong interpolation between some points. This probably due to different sampling rates for the datasets used as inputs, and these points is therefore neglected in the interpretation of the results.

The interpreted laminated sand-shale zones mainly plots along the laminated shale line, between the clean sand point and the shale point on the TS diagrams, as assumed from the R_v-R_h anisotropy interpretation. Zone 8 was initially interpreted as a dispersed shale zone, due to high shale volume and no separation between R_v and R_h above the OWC. According to the TS diagram, this zone plots along the laminated line and shows no signs of dispersed shale. This interpretation is therefore decided to be erroneous and the zone is processed as a laminated shaly sand zone in the summary section, using Archie's equation for saturation calculations. If a dispersed shale zone was present, an equation including shale volume, such as the Indonesian equation, would have been applied. Further on, the interpreted clean sand and shale zones are plotted around the endpoints, and correlates good with the zonation. No zones are plotted towards the dispersed endpoint.

The T2 distribution for well 7220/8-1, displayed in Appendix A.12, clearly shows the distribution forms described in Chapter 2.4.3 for shale and sand, and is therefore considered as a reliable input for both the DMR porosity and the R_{cg} calculation.

The DMR porosity calculated shows an excellent correlation with the core porosities in the gas zone (see Figure 16). As stated in Chapter 3.5, the TCMR and PHIT_D logs also shows a separation in the same zone due to incorrect readings, and the DMR porosity curve plots in between. This separation correlates with the ND separation. This indicates the DMR calculations fulfilled the purpose of correcting porosity in the gas zone without doing any gas corrections. The DMR porosity also shows good correlation with core porosity throughout the whole reservoir section.

The R_{cg} resistivity calculated for the coarse grained layers correlates good with the vertical resistivity throughout the reservoir intervals, which is a more accurate approximation in the hydrocarbon bearing, laminated zones (see example in Figure 15). As the vertical resistivity provides an average resistivity value over the thin beds of shale and HC filled sand, the real sand resistivity will be slightly larger in reality. The cut-offs for the T2 distributions seems to provide a shale volume fraction that correlates well with the fine and coarse grained zones. As stated in Chapter 3.5, the R_{cg} resistivity shows an improved resistivity and makes the conductive shale effects lessen due to the use of triaxial resistivities and T2 distributions.

The summary results (see Table 7) provides an overview over the hydrocarbon intervals present in well 7220/8-1. The results are based on the resistivity calculation result, R_{cg}, and the DMR porosity. This summary result is therefore considered to be correct in the shaly-sand and clean sand zones. If a result for the shales was desired, the resistivity for the fine grained layers, R_{fg}, had to have been used. The DMR porosity is assumed to be applicable throughout the whole reservoir section, due to good correspondence with the core porosities.

The total hydrocarbon pore thickness of 22.8 m seems reasonable considering the amount of shale within the reservoir section of 120.0 m. From Figure 19 it can be observed that the final water saturation is low throughout the whole reservoir section in well 7220/8-1, and hydrocarbons are filling up most of the pore (green colour fill) space. The water saturation seems to increase with increasing shale volume, which indicates that most of the water detected is irreducible shale water. As stated in Chapter 1, this laminated sand-shale reservoir is likely to produce oil and gas with a low water cut.

5.2 Potential Errors

- From the datasets given for well 7220/8-1, 7220/7-1 and 7220/5-1, logs containing the same data appears more than one time due to several logging runs in the well. The data saved in the harmonized dataset is considered the best data for this evaluation, but errors due to wrong choice of data could occur. Parameters, such as formation temperature, could vary when logging over a certain amount of time, and hence provide some differences in the metrics for each logging run.
- As the shale consist of different minerals, such as clay and quartz, anisotropy within the shale layers will exist. This implies that the anisotropy measured over a thin-bedded section of sand and shale could have higher anisotropy than just the indications for sand and shale laminas. R_v and R_h measured within the nearby shale formations in the wells, shows small indications of anisotropy. The shale laminas within the shaly sand intervals are therefore considered to have a limited impact on the total anisotropy result in this project.
- Due to R_{cg} result providing no solution in some intervals of the clean sand in well 7220/8-1, an error in this equation is present. Parameters in the second term of the equations provide negative numbers inside the square root, which lead to the incontinuity of the log through zone 4. This most likely due to unrealistically high log values for R_v and R_h.

5.3 Proposed Further Work

For further study of the reservoir in well 7220/8-1, a permeability study form TVD formation pressure points, NMR and core data is proposed. Due to the close relationship between porosity and permeability, improved information about the reservoir quality could be obtained by plotting the two parameters together and observe trends and variations.

For further study of the thin beds of sand and shale, core photos and high resolution image logs could be applied to the interpretation, in order to visualize and get a better knowledge of the location and extent of the beds. More data for the correlation wells, as T2 distributions, is also proposed in order to provide an even more precise lithology and fluid interpretation of the reservoir interval.

6. Conclusion

- Based on the result and discussion regarding the conventional analysis, well correlations and Thomas-Stieber diagrams, the zonation of reservoir fluids, lithology and shale distribution in well 7220/8-1 are considered as correct and suitable for use in further interpretations and calculations.
- The DMR porosity calculation provides a good match with core porosities. The method corrected for both NMR and density porosity in the gas zone, and correlates with the same porosity logs throughout the reservoir. This method will provide a corrected porosity without applying gas corrections to density porosity or slow down NMR logging speed for full polarization.
- The R_{cg} resistivity provides a result quite similar to the vertical resistivity in the laminated zones in well 7220/8-1. This result represents an estimate based on triaxial measurements and will thus provide a resistivity closer to the sand lamina resistivity than the apparent resistivity, due to removal of conductive shale dominance. This result is hence representative for the hydrocarbon filled sand laminas within the laminated reservoir sections. The laminated, low resistivity pay zones present in the reservoir, is no longer overlooked or underestimated.
- With the use of the DMR porosity, R_{cg} resistivity and zonation results, the thin bed and gas issues for the reservoir in well 7220/8-1 are solved. A corrected saturation is calculated from these results and provides an improved estimate for the total hydrocarbon pore thickness. In addition, the final water saturation result implies that a low water cut in the production of hydrocarbons is likely.

REFERENCES

ANDERSON, B., BARBER, T., LEVERIDGE, R., BASTIA, R., SAXENA, K. R., TYAGI, A. K., CLAVAUD, J.-B., COFFIN, B., DAS, M., HAYDEN, R., KLIMENTOS, T., MINH, C. C. & WILLIAMS, S. 2008. Triaxial induction—A new angle for an old measurement. pp. 64-84.

BRANDSEN, H. 2016. Shale and Clay Part II. *NTNU Lecture Notes: Petrophysics, Interpretation of Well Data, Advanced Course*.

COATES, G. R., XIAO, L. & PRAMMER, M. G. 1999. *NMR logging: principles and applications*, Haliburton Energy Services.

FREEDMAN, R., MINH, C. C., GUBELIN, G., FREEMAN, J., MCGINNESS, T., TERRY, B. & RAWLENCE, D. Combining NMR and density logs for petrophysical analysis in gas-bearing formations. SPWLA 39th Annual Logging Symposium, 1998. Society of Petrophysicists and Well-Log Analysts.

KENNEDY, M. 2015. *Practical petrophysics*, Elsevier.

NPD. 2014. *Lithostratigraphic Chart Norwegian Sea* [Online]. Available: http://www.npd.no/Global/Engelsk/2-Topics/Geology/Lithostratigraphy/BH-OD1409003.pdf [Accessed 02.06.2016 2016].

NPD. 2016a. *Factmaps* [Online]. Available: http://gis.npd.no/factmaps/html_20/ [Accessed 29.04.2016].

NPD. 2016b. *NORDMELA FM* [Online]. Available: http://factpages.npd.no/ReportServer?/FactPages/PageView/strat_Litho_level1_group_formation&rs:Command=Render&rc:Toolbar=false&rc:Parameters=f&NpdId=118&IpAddress=129.241.65.212&CultureCode=en [Accessed 02.06.2016 2016].

NPD. 2016c. *STØ FM* [Online]. Available: http://factpages.npd.no/ReportServer?/FactPages/PageView/strat_Litho_level1_group_formation&rs:Command=Render&rc:Toolbar=false&rc:Parameters=f&NpdId=159&IpAddress=129.241.65.212&CultureCode=en [Accessed 02.06.2016 2016].

NPD. 2016d. *Well 7220/5-1* [Online]. Available: http://factpages.npd.no/factpages/Default.aspx?culture=no [Accessed 29.04.2016].

NPD. 2016e. *Well 7220/7-1* [Online]. Available: http://factpages.npd.no/factpages/Default.aspx?culture=no [Accessed 29.04.2016].

NPD. 2016f. *Well 7220/8-1* [Online]. Available: http://factpages.npd.no/factpages/Default.aspx?culture=no [Accessed 29.04.2016].

OLSEN, S. G. 2015. Petrophysical Thin-Bed Reservoir Evaluation of Well 7220/8-1 using Triaxial Resistivity Data (unpublished). *NTNU*.

SCHLUMBERGER 1989. *Log Interpretation Principles/Applications*, Schlumberger Educational Services.

SCHLUMBERGER. 2009. *True 3D measurements for enhanced reservoir quantification - RT scanner* [Online]. Available: http://www.slb.com/~/media/Files/evaluation/brochures/wireline_open_hole/petrophysics/resistivity/rt_scanner_br.pdf [Accessed 05.11.2015 2015].

SCHLUMBERGER. 2015a. *Techlog* [Online]. Available: https://www.software.slb.com/products/techlog [Accessed 10.11.15 2015].

SCHLUMBERGER 2015b. *Techlog Fundementals and Conventional Log Analysis*.

SCHLUMBERGER. 2015c. *Techlog Petrophysics* [Online]. Available: https://www.software.slb.com/products/techlog/techlog-petrophysics [Accessed 10.11 2015].

SHRAY, F. & BORBAS, T. Evaluation of laminated formations using nuclear magnetic resonance and resistivity anisotropy measurements. SPE Eastern Regional Meeting, 2001. Society of Petroleum Engineers.

SKOGEN, E. 2013. Nuclear Magnetic Resonance. *NTNU lecture notes: Petrophysics - Well Logging, Fundamentals*.

THOMAS, E. C. & STIEBER, S. J. The distribution of shale in sandstones and its effect upon porosity. SPWLA 16th annual logging symposium, 1975. Society of Petrophysicists and Well-Log Analysts.

TYAGI, A. K., BASTIA, R. & DAS, M. Identification and Evaluation of the Thin Bedded Reservoir Potential in the East Coast Deep Water Basins of India. 7 th International Conference and Exposition on Petroleum Geophysics, SPG, Hyderabad, 2008.

APPENDIX

A.1 Core Data for Well 7220/8-1

Depth	Phi_Core	Grain Density		Depth	Phi_Core	Grain Density		Depth	Phi_Core	Grain Density
1293,15	0,289	2,64		1331,01	0,265	2,64		1368,03	0,141	2,63
1294,02	0,034	2,65		1332,01	0,264	2,63		1369,03	0,297	2,62
1295,02	0,257	2,64		1333,01	0,282	2,63		1370,03	0,241	2,64
1296	0,245	2,64		1334,01	0,282	2,64		1371,02	0,204	2,63
1298,01	0,26	2,64		1335,01	0,272	2,63		1372,03	0,254	2,63
1299,01	0,262	2,64		1336,01	0,258	2,63		1373,02	0,247	2,65
1300,01	0,255	2,63		1337,01	0,299	2,64		1374,02	0,263	2,63
1301,01	0,255	2,64		1338,01	0,286	2,63		1375,02	0,163	2,61
1302,01	0,258	2,63		1339,01	0,311	2,63		1376,02	0,028	2,63
1303,01	0,269	2,64		1340,01	0,31	2,64		1377,02	0,117	2,66
1304,01	0,224	2,65		1341,01	0,294	2,64		1379,02	0,097	2,67
1305,01	0,235	2,64		1342,01	0,312	2,64		1380,02	0,274	2,64
1306,01	0,24	2,63		1343,01	0,294	2,63		1381,02	0,28	2,63
1307,01	0,227	2,64		1344,01	0,306	2,65		1382,02	0,284	2,63
1308,01	0,229	2,65		1345,01	0,348	2,65		1383,02	0,295	2,63
1309,01	0,216	2,64		1346,01	0,333	2,64		1384,05	0,311	2,62
1310,01	0,205	2,64		1347,01	0,305	2,64		1385,03	0,241	2,65
1311,01	0,195	2,65		1348,08	0,3	2,63		1386,05	0,023	2,65
1312,01	0,231	2,63		1349,01	0,294	2,64		1387,05	0,292	2,63
1313,01	0,205	2,63		1350,01	0,315	2,65		1388,03	0,297	2,62
1314,01	0,212	2,64		1351,19	0,32	2,64		1389,02	0,276	2,62
1315,01	0,209	2,64		1352,01	0,271	2,65		1390,02		
1316,01	0,003	2,68		1353,01	0,266	2,64		1391,02	0,272	2,62
1317,01	0,255	2,63		1354,01	0,264	2,63		1392,02	0,168	2,63
1318,01	0,267	2,65		1355,01	0,288	2,66		1393,02	0,278	2,61
1319,01	0,258	2,65		1356,01	0,3	2,64		1394,03	0,248	2,62
1320,01	0,251	2,64		1357,04	0,255	2,63		1395,02	0,226	2,61
1321,08	0,274	2,63		1358,02	0,295	2,62		1396,02	0,163	2,66
1322,01	0,272	2,66		1359,07	0,252	2,63		1397,02	0,26	2,61
1323,01	0,271	2,64		1360,03				1398,03	0,271	2,62
1324,05	0,264	2,64		1361,02	0,273	2,64		1399,02	0,282	2,61
1325,01	0,257	2,64		1362,02	0,282	2,62		1400,02	0,229	2,62
1326,01	0,258	2,64		1363,02	0,275	2,62		1401,02	0,224	2,73
1327,01	0,275	2,64		1364,02	0,238	2,66		1402,02	0,143	2,63
1328,01	0,274	2,64		1365,04	0,273	2,64		1403,02	0,302	2,63
1329,01	0,271	2,64		1366,02				1404,02	0,28	2,61
1330,01	0,273	2,63		1367,03	0,285	2,63				

A.2 Schlumberger Interpretation Chart for Water Density

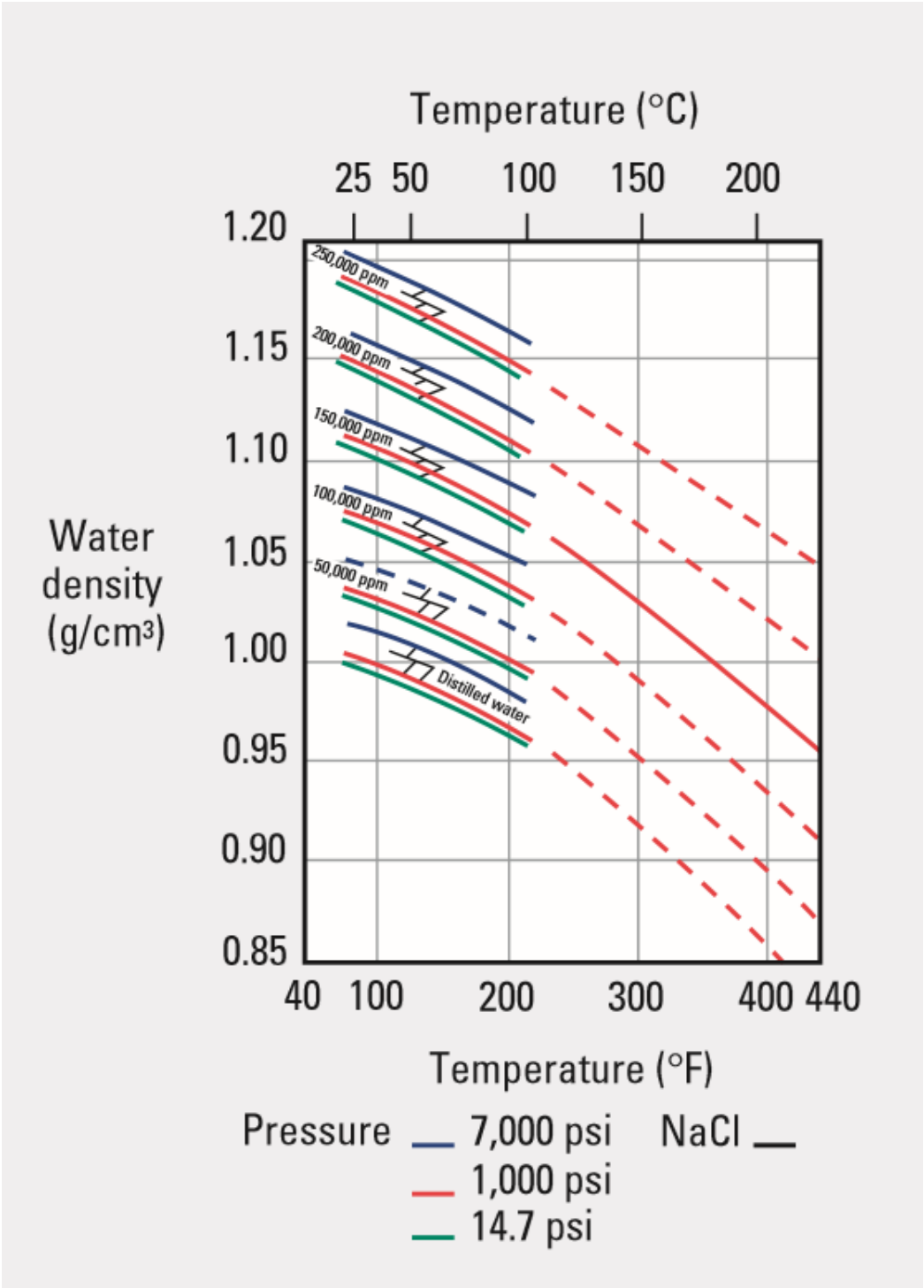

A.3 TVD vs. Formation Pressure Plot for Well 7220/8-1

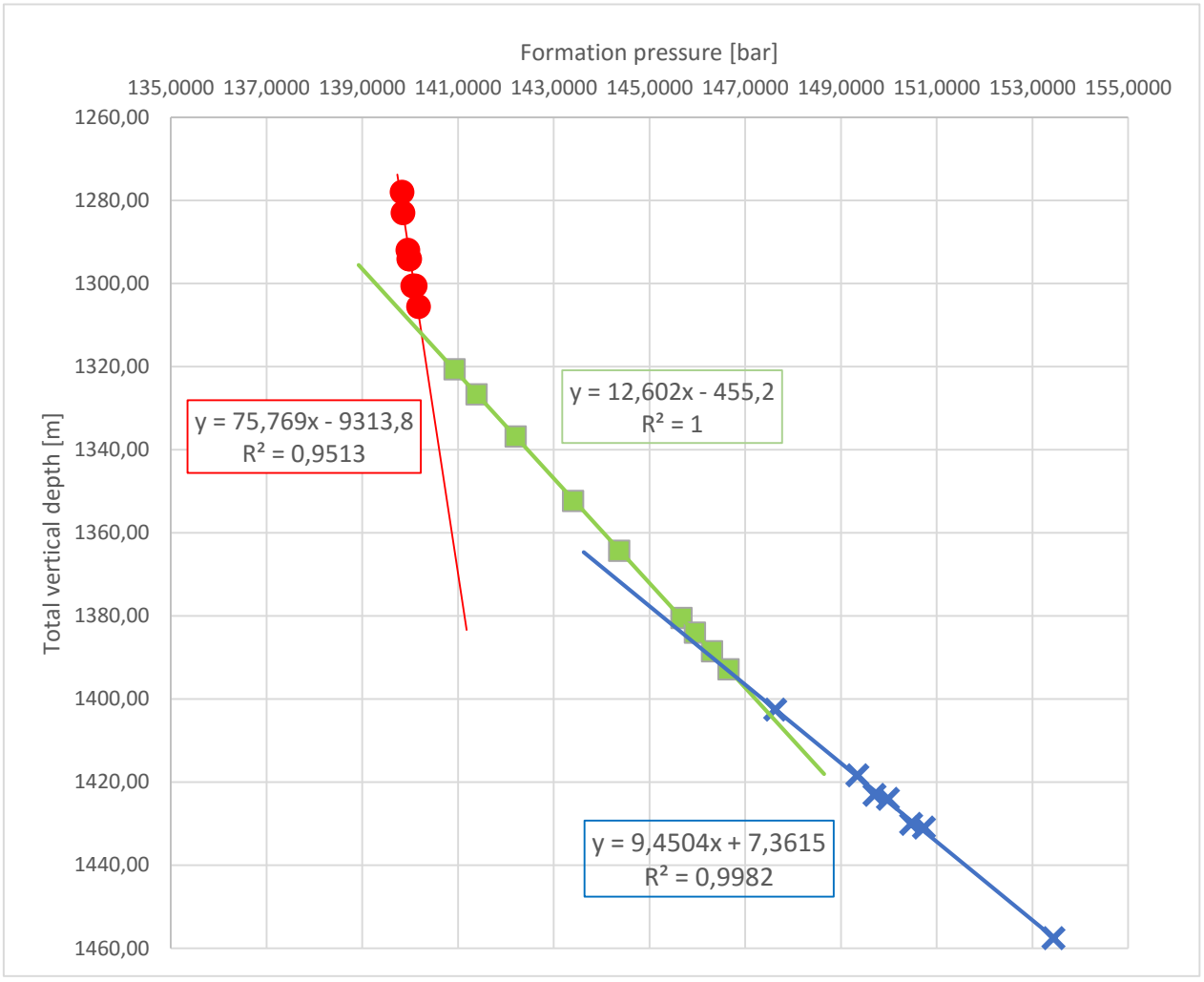

A.4 Formation Pressure Table Well 7220/8-1

Test	File	Measured Depth M	True Vertical Depth M	Drawdown Mobility mD/cP	Mud pressure Before BAR	Mud pressure After BAR	Last read build−up Pressure BAR	Formation Pressure BAR	Test type
2	196	1278,01	1278,01	43,42	153,3732	153,2707	139,8339	139,8339	Volumetric Limited Draw-down
4	197	1282,99	1282,99	141,12	153,8854	153,8621	139,8514	139,8514	Volumetric Limited Draw-down
5	198	1292	1292,00	393,08	155,0366	154,9443	139,9551	139,9551	Volumetric Limited Draw-down
7	199	1294,09	1294,09	1061,73	155,305	155,204	139,9762	139,9762	Volumetric Limited Draw-down
2	23	1294,11	1294,11	267,68	161,708	161,7474	139,9942	139,9942	Volumetric Limited Draw-down
4	24	1300,6	1300,60	515,42	162,5734	162,5708	140,1069	140,1069	Volumetric Limited Draw-down
9	200	1300,6	1300,60	1047,3	156,0486	156,0008	140,0573	140,0573	Volumetric Limited Draw-down
6	25	1305,6	1305,60	102,6	163,2263	163,2033	140,181	140,1810	Volumetric Limited Draw-down
8	26	1312,11	1312,11	28,13	164,0751	164,0572	140,3307	140,3307	Volumetric Limited Draw-down
37	46	1320,61	1320,61	386,7	165,0594	164,8469	140,9267	140,9267	Volumetric Limited Draw-down
10	27	1326,6	1326,60	1020,54	165,9236	165,9116	141,3873	141,3873	Volumetric Limited Draw-down
35	43	1336,74	1336,74		167,2575	167,2114	142,2015	142,2015	Volumetric Limited Draw-down
12	28	1352,26	1352,26	2172,69	169,1448	169,1555	143,4029	143,4029	Volumetric Limited Draw-down
16	30	1364,26	1364,26	574,27	170,7036	170,6938	144,3652	144,3652	Volumetric Limited Draw-down
14	29	1374,45	1374,45	0,35	172,0271	172,0521	148,0575	148,0575	Volumetric Limited Draw-down
18	31	1380,46	1380,46	508,67	172,8351	172,8373	145,6633	145,6633	Volumetric Limited Draw-down
33	41	1383,96	1383,96	184,54	173,442	173,2616	145,9458	145,9458	Volumetric Limited Draw-down
20	32	1388,46	1388,46	4,69	173,8647	173,8712	146,306	146,3060	Volumetric Limited Draw-down
28	38	1392,8	1392,80	4,29	174,4692	174,5086	146,6464	146,6464	Volumetric Limited Draw-down
22	33	1402,52	1402,52	843,72	175,7292	175,7329	147,625	147,6250	Volumetric Limited Draw-down
31	40	1418,36	1418,36	363,82	177,8563	177,8558	149,3428	149,3428	Volumetric Limited Draw-down
30	39	1419,54	1419,54	2,96	177,9509	177,9921	149,9714	149,9714	Volumetric Limited Draw-down
27	106	1423,97	1423,08	781,98	170,0155	170,0067	149,7006	149,7006	Volumetric Limited Draw-down
24	34	1424,01	1424,01	80,97	178,5211	178,5281	149,9792	149,9792	Volumetric Limited Draw-down
25	105	1430,96	1430,07	406,34	170,8549	170,8641	150,4633	150,4633	Volumetric Limited Draw-down
26	35	1430,96	1430,96	136,25	179,431	179,4388	150,7322	150,7322	Volumetric Limited Draw-down
23	104	1458,47	1457,56	1371,64	174,1849	174,1804	153,4402	153,4402	Volumetric Limited Draw-down
21	103	1518,8	1517,89	609,65	181,4682	181,4567	160,0081	160,0081	Volumetric Limited Draw-down
19	101	1725	1724,09	211,16	206,3629	206,3544	182,4842	182,4842	Volumetric Limited Draw-down
15	99	1789,51	1788,60	3,86	214,1401	214,1205	189,5056	189,5056	Volumetric Limited Draw-down
17	100	1791,51	1790,60	143,13	214,3559	214,3473	189,7231	189,7231	Volumetric Limited Draw-down
12	98	1884,5	1883,60	97,1	225,5194	225,5128	199,8586	199,8586	Volumetric Limited Draw-down
10	96	2016,01	2015,10	62,97	241,2822	241,2633	214,4279	214,4279	Volumetric Limited Draw-down
8	95	2129,5	2128,60	763,17	254,7243	254,7096	227,1476	227,1476	Volumetric Limited Draw-down
6	94	2141,49	2140,58	26,96	256,0598	261,1638	228,4636	228,4636	Volumetric Limited Draw-down
4	92	2151,1	2150,19	562,25	257,3036	257,2745	229,5149	229,5149	Volumetric Limited Draw-down

A.5 Schlumberger Interpretation Chart for Resistivity of NaCl Water Solutions

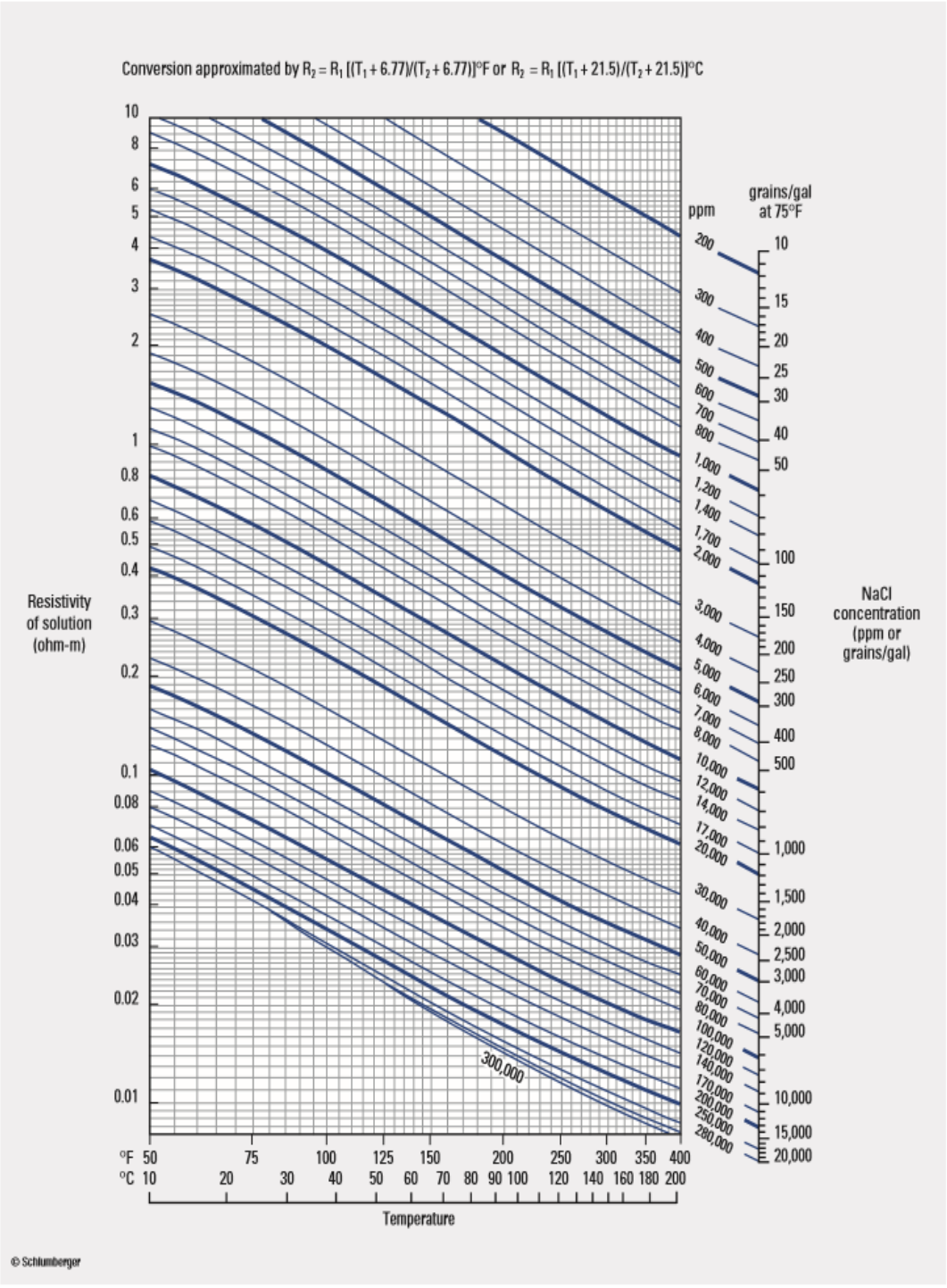

A.6 Schlumberger Interpretation Chart for Consentration of NaCl Solutions

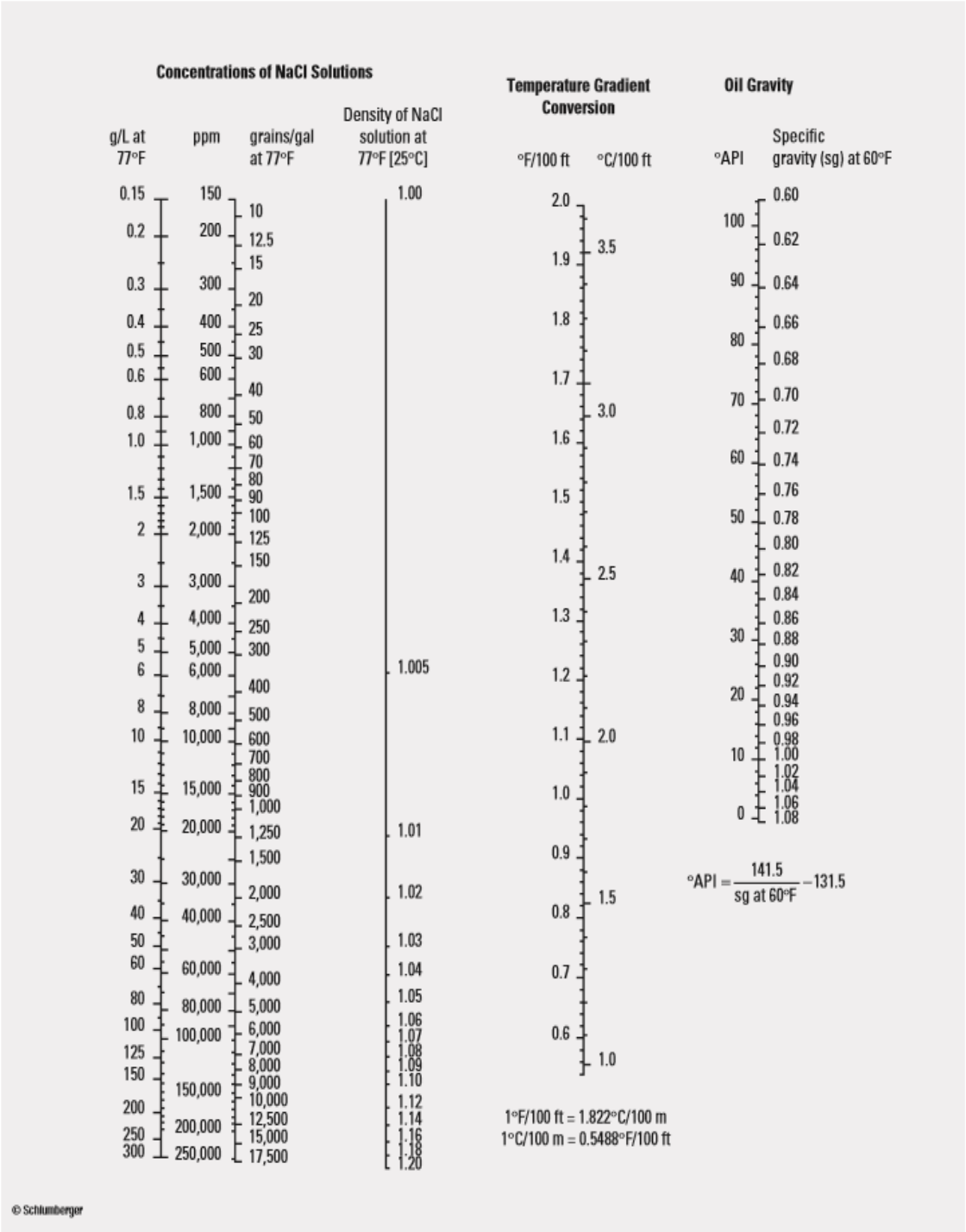

A.7 Field Print Well 7220/8-1

Schlumberger

Company: **Statoil**

Well: **7220/8−1**
Field: **Skrugard**
Rig: **Polar Pioneer** Country: **Norway**

HRLA−PEX−GR
High Resolution Laterlog Array
1:200

Rig: Polar Pioneer
Field: Skrugard
Location: Barents Sea, Norwegian Sector
Well: 7220/8−1
Company: Statoil

LOCATION

Barents Sea, Norwegian Sector	Elev.: K.B.	23.00 m
UTMN: 8044087 m	G.L.	−374.00 m
UTME: 477634 m	D.F.	23.00 m
Permanent Datum: Mean Sea Level	Elev.:	0.00 m
Log Measured From: Drill Floor	23.00 m	above Perm. Datum
Drilling Measured From: Drill Floor		

Rig: Polar Pioneer	Max. Well Deviation 3.19 deg	Longitude 20° 20' 2.25" E	Latitude 72° 29' 28.95" N

Logging Date			23−Apr−2011				
Run Number			3A				
Depth Driller			2222.33 m				
Schlumberger Depth			2220 m				
Bottom Log Interval			2213 m				
Top Log Interval			1249.5 m				
Casing Driller Size @ Depth			7.000 in @ 1251 m			@	
Casing Schlumberger			1249.5 m				
Bit Size			6.000 in				
Type Fluid In Hole			KCL/Polymer Spec 3d WBM				
MUD	Density	Viscosity	1.21 g/cm3				
MUD	Fluid Loss	PH					
MUD	Source Of Sample		Shakers				
RM @ Measured Temperature			0.170 ohm.m @ 23 degC			@	
RMF @ Measured Temperature			0.149 ohm.m @ 23 degC			@	
RMC @ Measured Temperature			0.770 ohm.m @ 23 degC			@	
Source RMF	RMC		Press	Press			
RM @ MRT	RMF @ MRT		0.098 @ 56	0.086 @ 56		@	@
Maximum Recorded Temperatures			56 degC	56	56		
Circulation Stopped	Time		22−Apr−2011		11:20		
Logger On Bottom	Time		24−Apr−2011		0:35		
Unit Number	Location		625	NOBO			
Recorded By			P.Dorehill/O. Bautista				
Witnessed By			T. Kuklina/M. Hamer				

A.8 CMR Depth Log Report for Well 7220/8-1

Input DLIS Files

	CMR_ECS_TLD_MCFL_186LUP	FN:321		28−Apr−2011 14:07	1432.6 M	1211.6 M

Output DLIS Files

DEFAULT	CMR_ECS_TLD_MCFL_186PUP	FN:14	PRODUCER	17−Jul−2011 23:14	1432.6 M	1211.9 M
CUSTOMER	CMR_ECS_TLD_MCFL_186PUC	FN:15	CUSTOMER	17−Jul−2011 23:14	1432.6 M	1211.9 M

CMR DEPTH LOG REPORT

PARAMETER SUMMARY

Tool Type: CMR−Plus	Cart. Number: 294	Sonde Number: 277	
Kit Number: 28	DHC Version : 17.2	DSP Version : 14	SP Version : 10182006
Mode: Expert Depth Log − B Mode		LFST Freq(khz) : 2215	LFST Temp(degc) : 38.75
Log Direction: Up	Polarization Correction: On	EPM: Yes	EPM T1/T2: Auto
Despiking: Off	High Res: Off	KBFV: Off	DMRP: Off
Echo Spacing(us):	(200 200)		
Polarization Times(sec) for:	T1=1s: (infinity 0.02)	T1=3s: (infinity 0.02)	T1=5s: (infinity 0.02)
Number of Echoes:	(3000 30)		
Repetition:	(1 10)	Duty Cycle (highest): 0.0282	
Regularization:	Auto		
T2 Min(msec): 0.3	T2 Max(msec): 3000	T2 Cutoff(msec): 33	T1/T2: 1.5
Number of Components: 30	Downhole Stacking: 3	Uphole Stacking: 1	First Echo Used: No
Multiple T2 Cutoffs(msec):	(0.3 1 3 10 33 100 300 1000 3000)		
Sample Int.(in): 7.5	Req Log Speed (f/h): 400		

A.9 Schlumberger Interpretation Chart for Longitudinal (Bulk) Relaxation Time of Methane

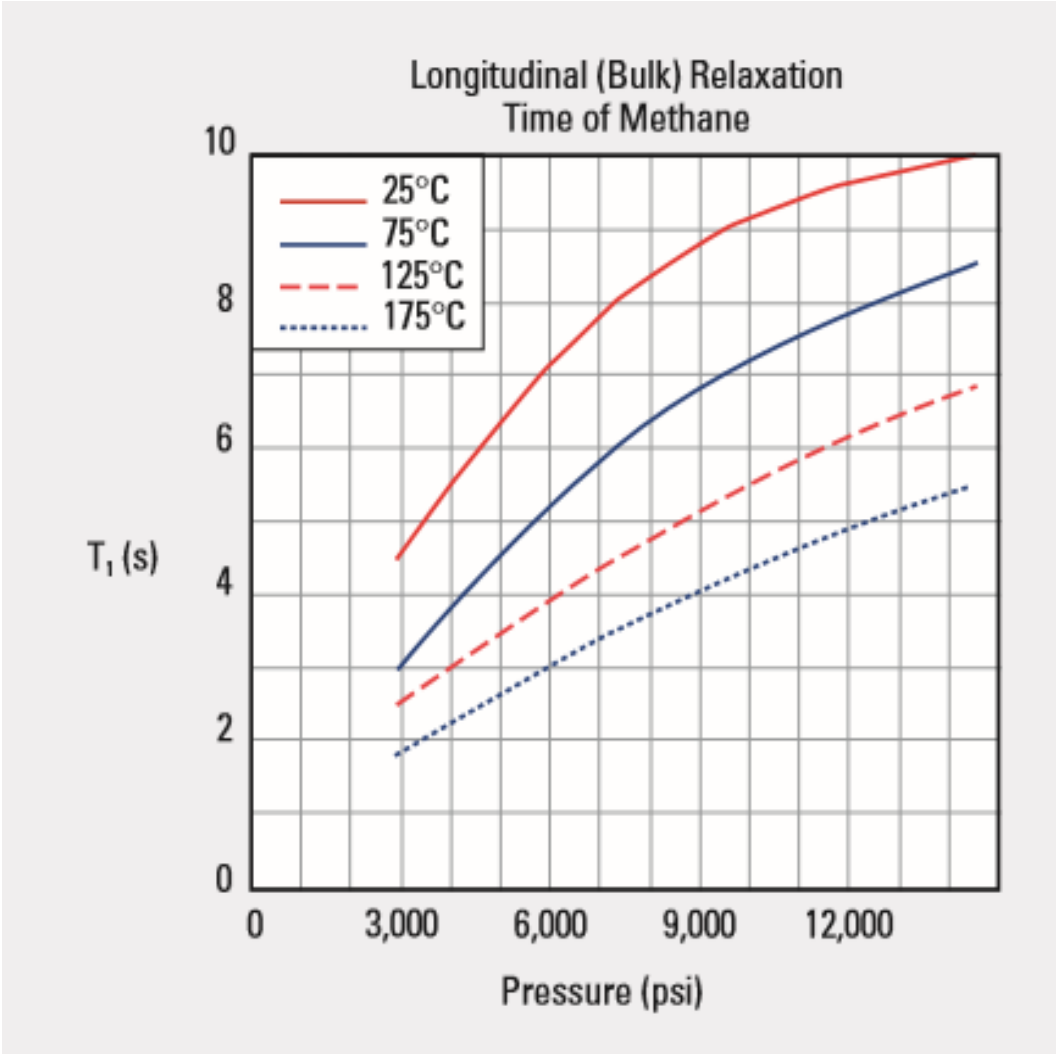

A.10 Schlumberger Interpretation Chart for Hydrocarbon Index for Gas

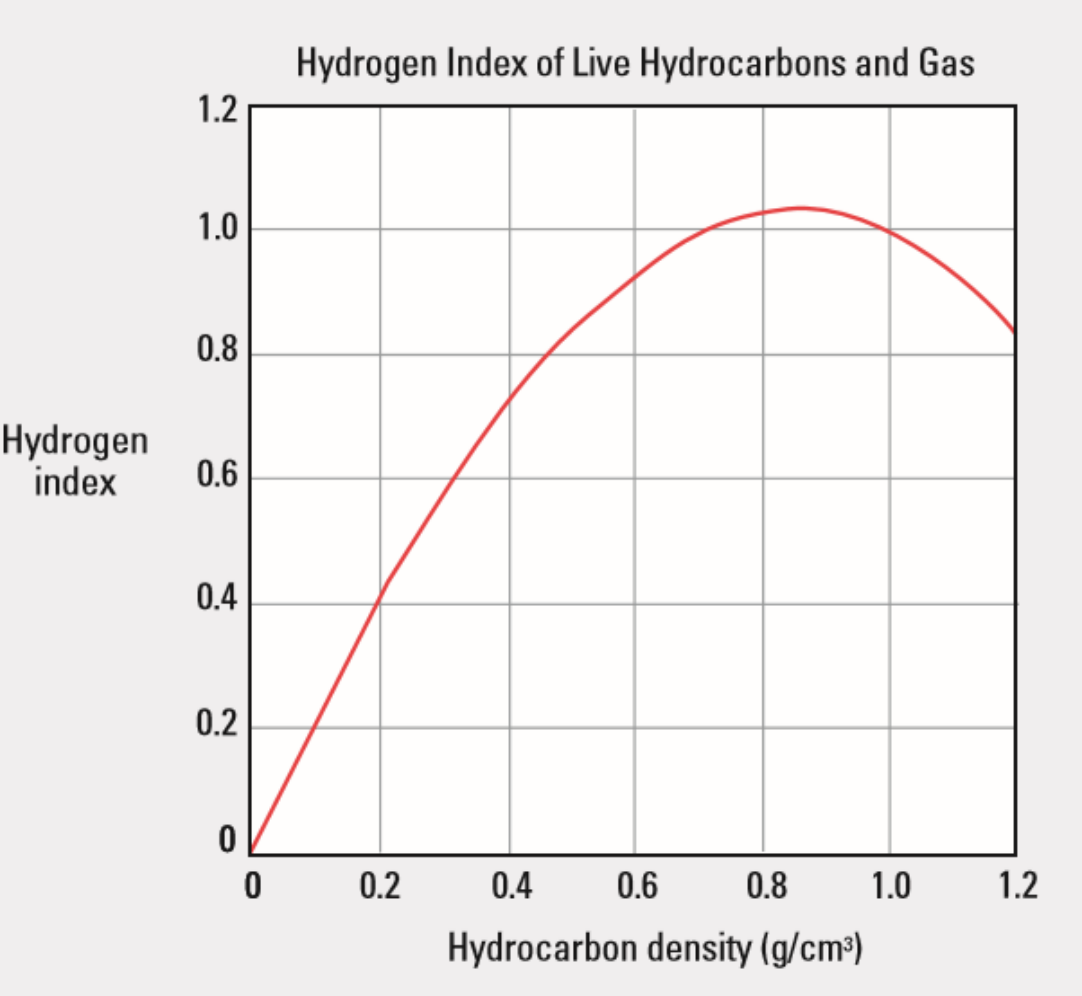

A.11 Zonation of Well 7220/8-1

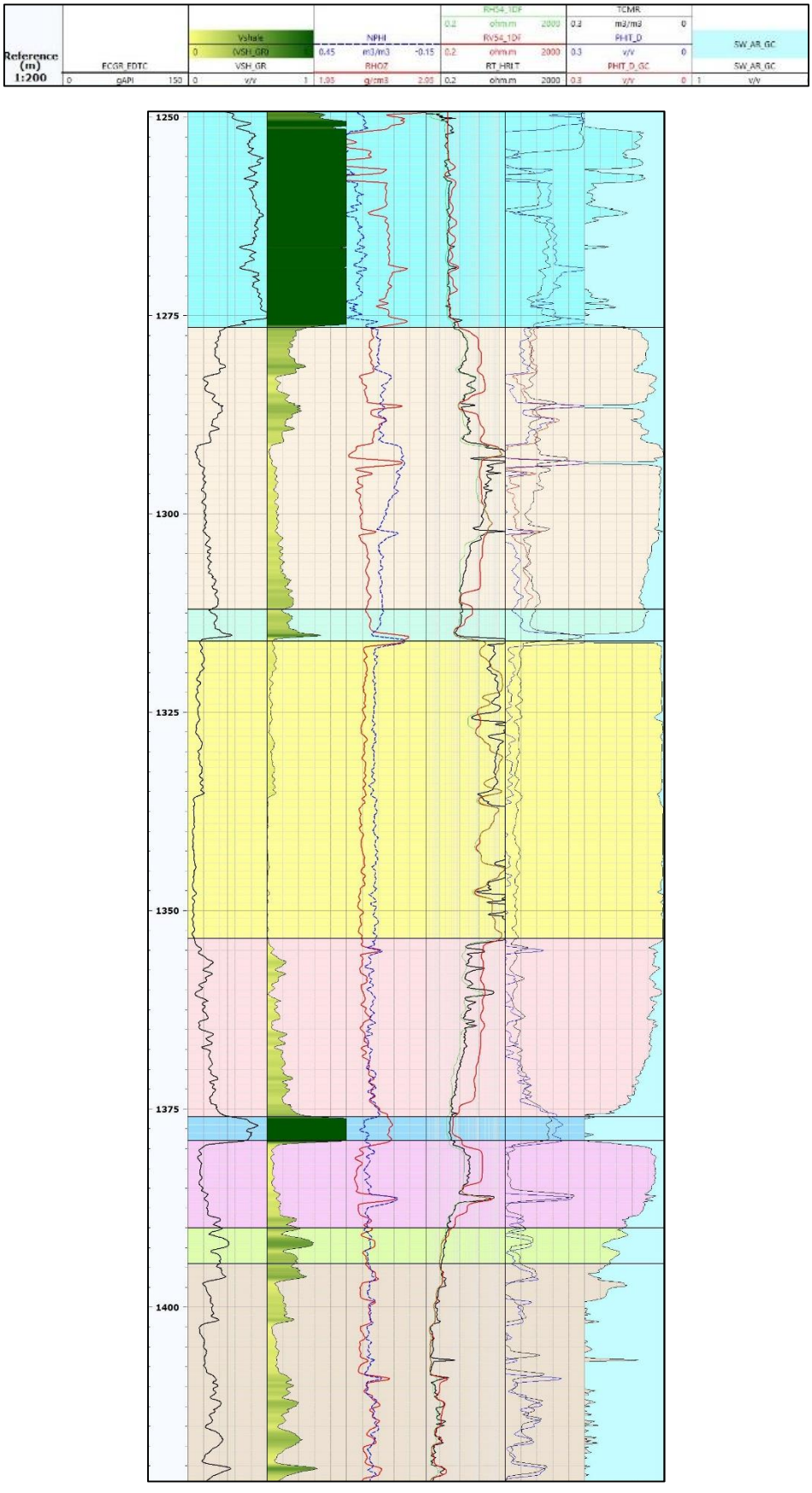

A.12 Log Data and Conventional Results for Well 7220/8-1

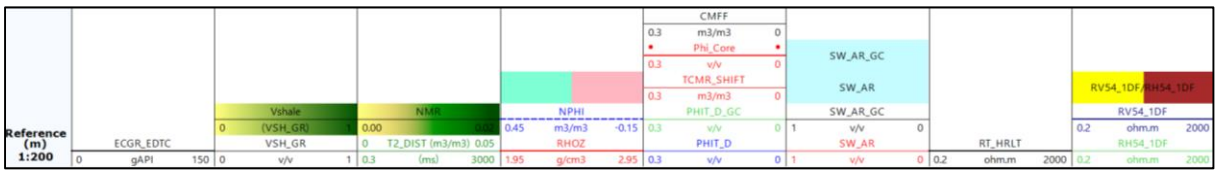

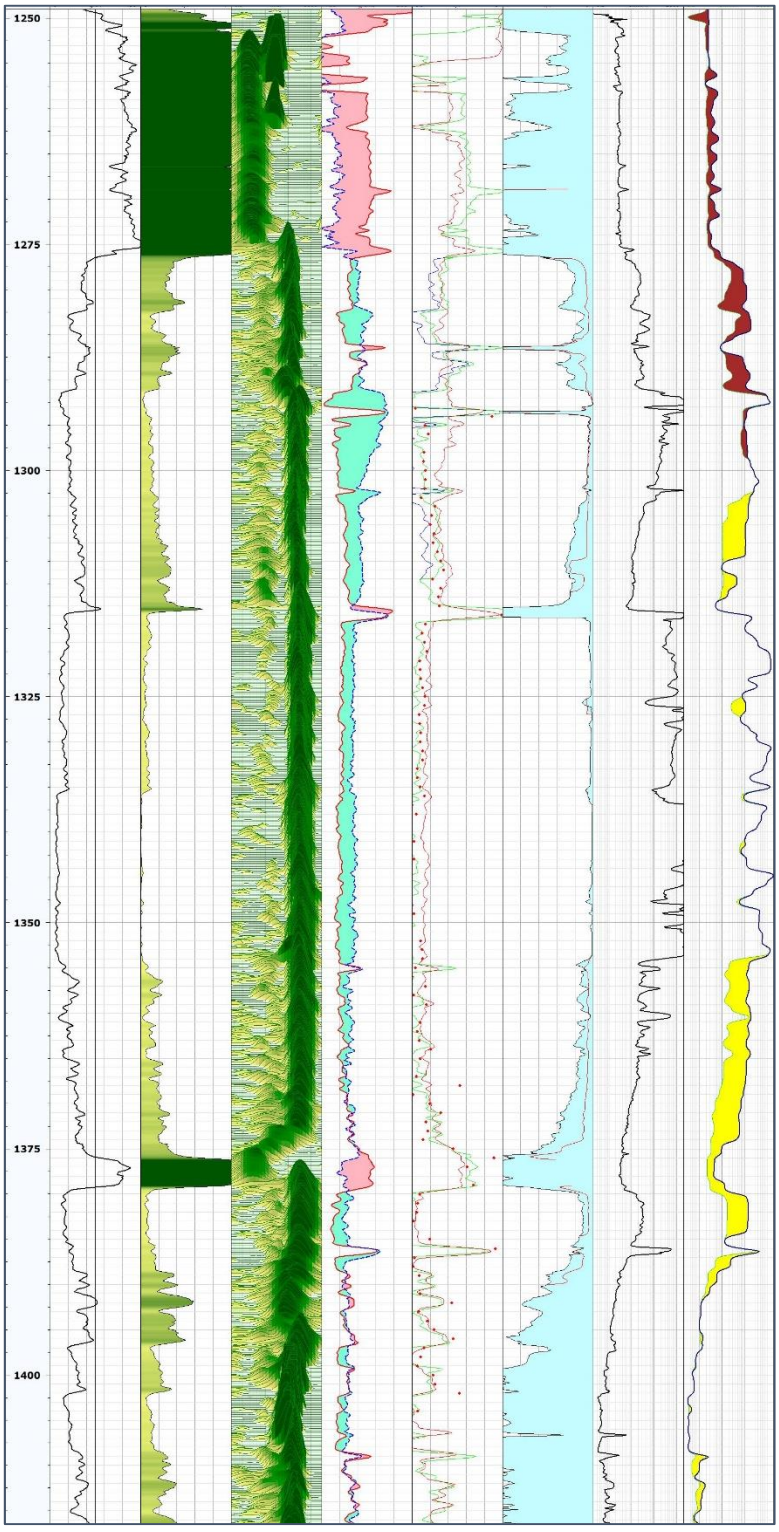

A.13 Log Data and Conventional Results for Well 7220/5-1

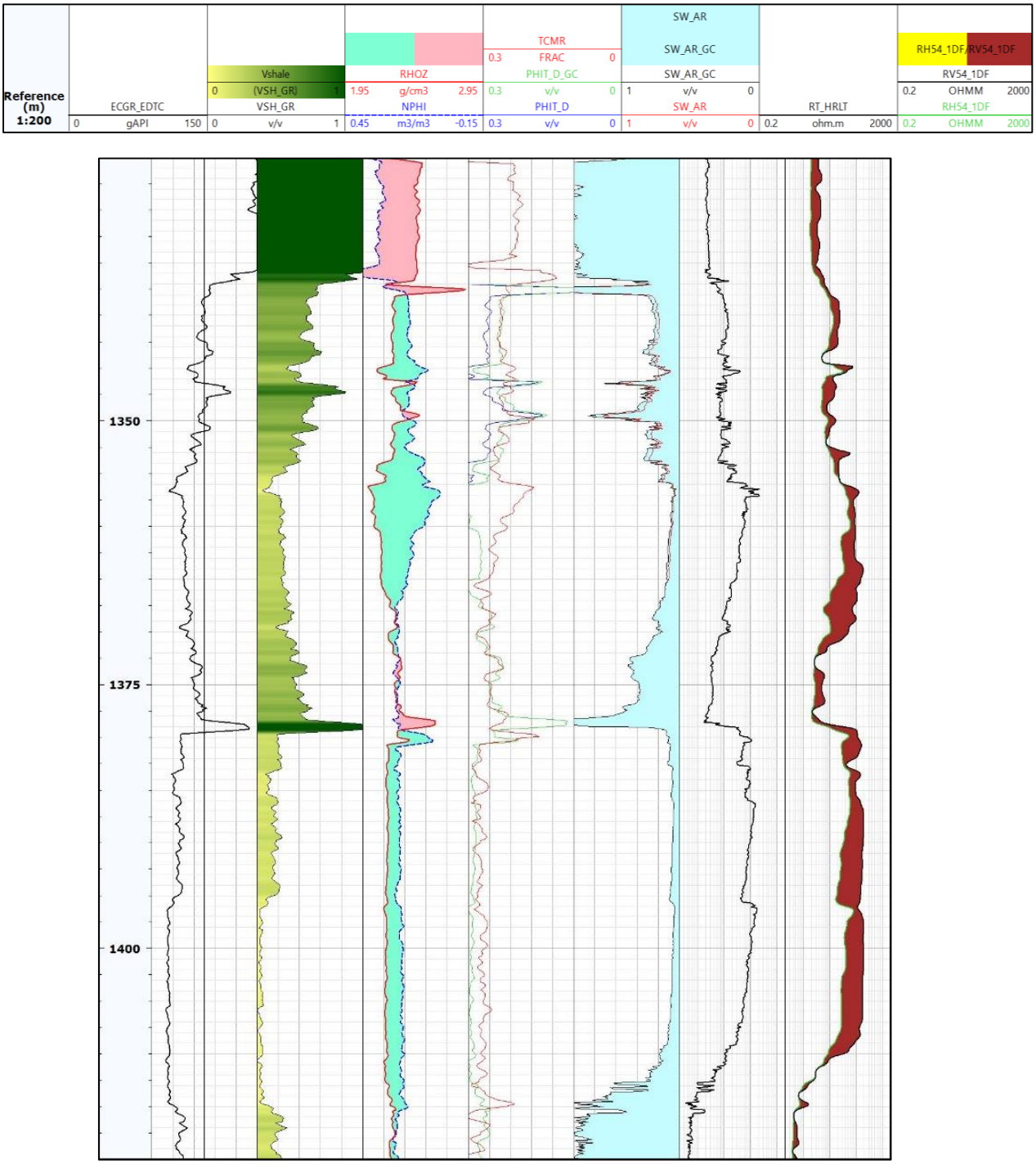

A.14 Log Data and Conventional Results for Well 7220/7-1

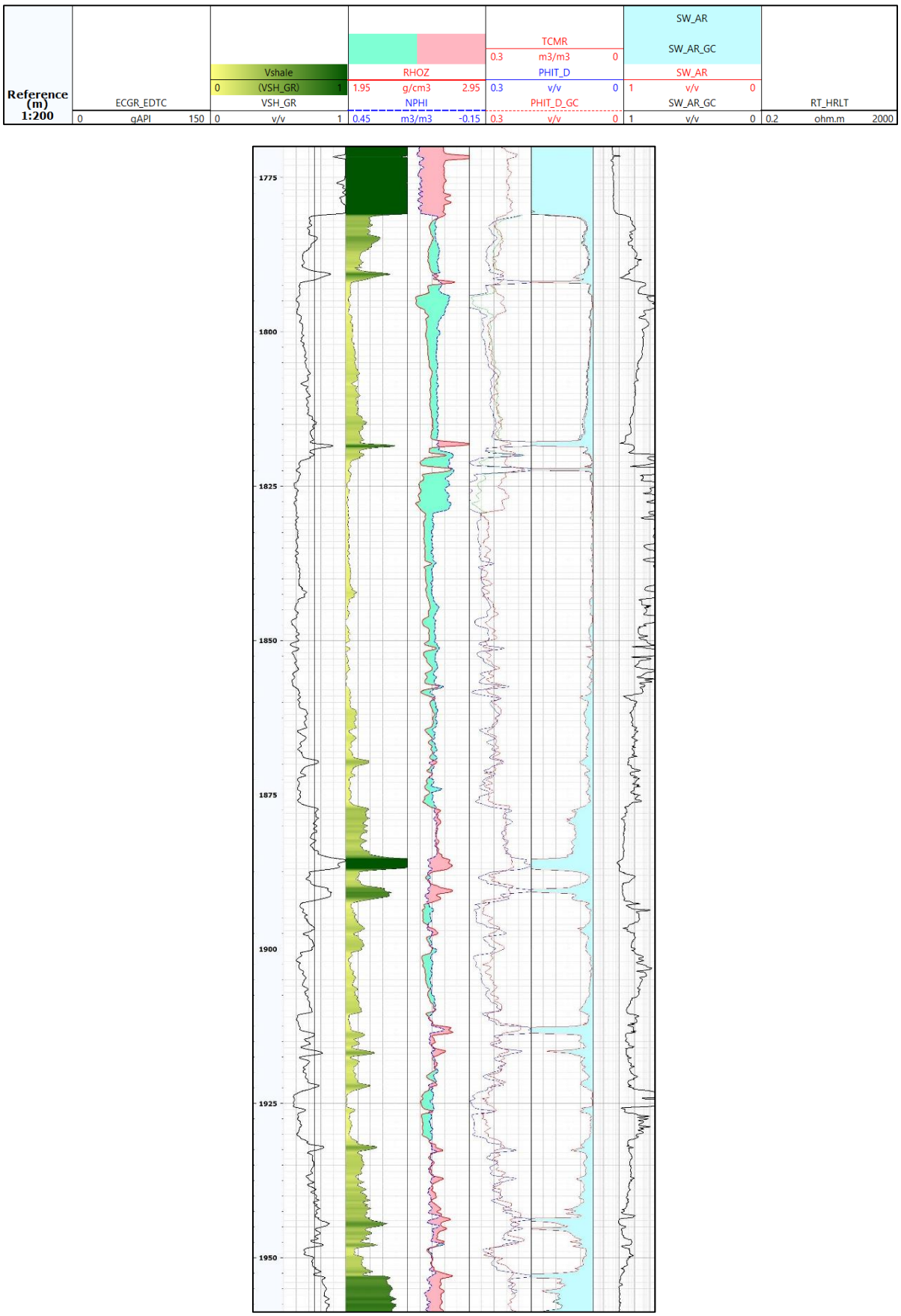

A.15 Results for DMR and Rcg vs. Conventional Logs and NMR Data in Well 7220/8-1

		Phi_Core				RH54_1DF
		0.4 v/v 0				0.2 ohm.m 2000
		PHIT_D				RT_HRLT
		0.4 v/v 0				0.2 ohm.m 2000
	Vshale	DMR	NPHI		NMR	RV54_1DF
Reference (m) 1:200	0 (VSH_GR) 1	0.4 v/v 0	0.45 m3/m3 -0.15		0.00 0.02	0.2 ohm.m 2000
	VSH_GR	TCMR_SHIFT	RHOZ		0 T2_DIST (m3/m3) 0.05	Rcg_minus_corr
	0 v/v 1	0.4 m3/m3 0	1.95 g/cm3 2.95		0.3 (ms) 3000	0.2 ohm.m 2000

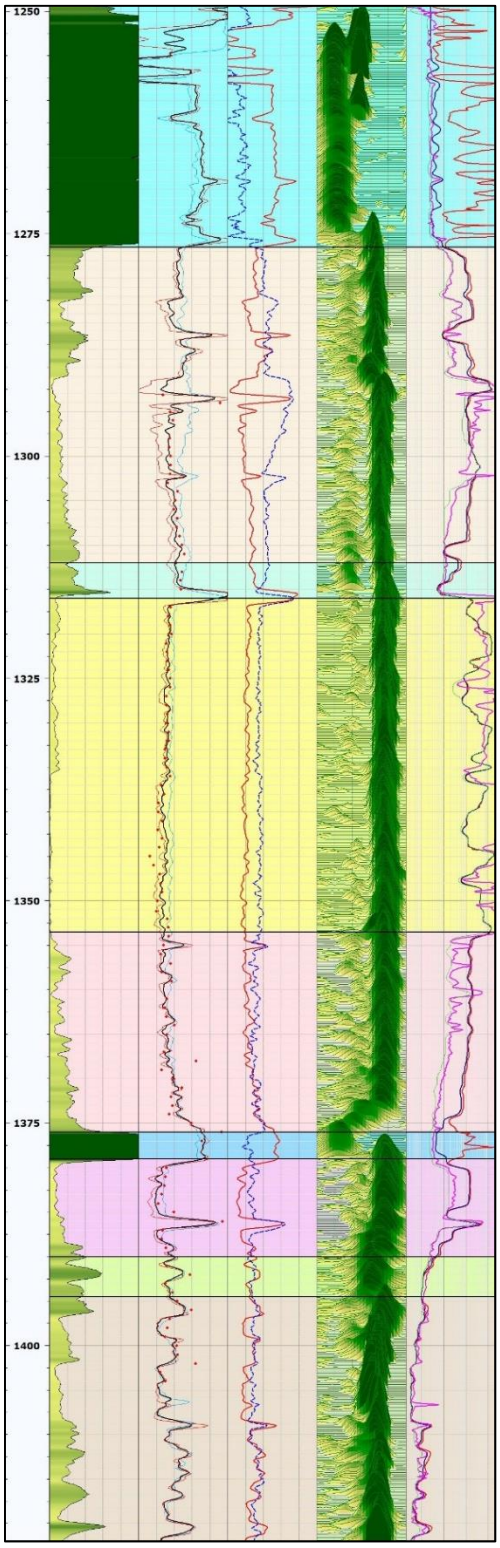

A.16 Formation Tops from NPD Factpages

Depth(m) (MD)	Well 7220/8-1		Depth(m) (MD)	Well 7220/7-1		Depth(m) (MD)	Well 7220/5-1
397	NORDLAND GP		405	NORDLAND GP		428	NORDLAND GP
455	SOTBAKKEN GP		485	SOTBAKKEN GP		478	SOTBAKKEN GP
455	TORSK FM		485	TORSK FM		478	TORSK FM
1014	ADVENTDALEN GP		1316	ADVENTDALEN GP		1035	ADVENTDALEN GP
1014	KOLMULE FM		1316	KOLMULE FM		1035	KOLMULE FM
1227	KOLJE FM		1710	KOLJE FM		1238	KNURR FM
1245	KNURR FM		1732	KNURR FM		1296	HEKKINGEN FM
1252	FUGLEN FM		1740	FUGLEN FM		1312	FUGLEN FM
1276	KAPP TOSCANA GP		1781	KAPP TOSCANA GP		1337	KAPP TOSCANA GP
1276	STØ FM		1781	STØ FM		1337	STØ FM
1354	NORDMELA FM		1857	NORDMELA FM		1415	NORDMELA FM
1511	TUBÅEN FM		2023	TUBÅEN FM		1578	TUBÅEN FM
1628	FRUHOLMEN FM		2130	FRUHOLMEN FM		1695	FRUHOLMEN FM
2122	SNADD FM						

A.17 Nomenclature

- NPD – The Norwegian Petroleum Directorate
- OWC – Oil-Water Contact
- OGC – Oil-Gas Contact
- TVD – Total Vertical Depth
- MD – Measured Depth
- GR – Gamma Ray
- ND – Neutron-Density
- HC – Hydrocarbon
- V_{sh} – Shale Volume
- Φ_t – Total Porosity
- Sw_AR – Archie Water Saturation
- Sw_AR_GC – Gas Corrected Archie Water Saturation
- Sw_AR_fin - Archie Water Saturation applying DMR and R_{cg} as Inputs
- BVW – Bulk Fluid Volume
- BVW_AR_fin – Bulk Fluid Volume from Archie's Equation Applying DMR and R_{cg} as Inputs
- PHIT_D – Density Porosity
- PHIT_D_GC – Gas Corrected Density Porosity
- TCMR – NMR Porosity
- TCMR_SHIFT – Depth Shifted NMR Porosity
- DMR – Density Magnetic Resonance
- HI – Hydrogen Index
- T1 – Longitudinal Relaxation Time
- T2 – Transverse Relaxation Time
- P_g – Gas Polarization Function
- W – Wait Time for CMPG Pulse Sequence
- R_{cg} – Resistivity of Coarse Grained Layer
- R_{fg} – Resistivity of Fine Grained Layer
- f_{Vcg} – Volume Fraction Coarse Grained Layer
- f_{Vfg} – Volume Fraction Fine Grained Layer